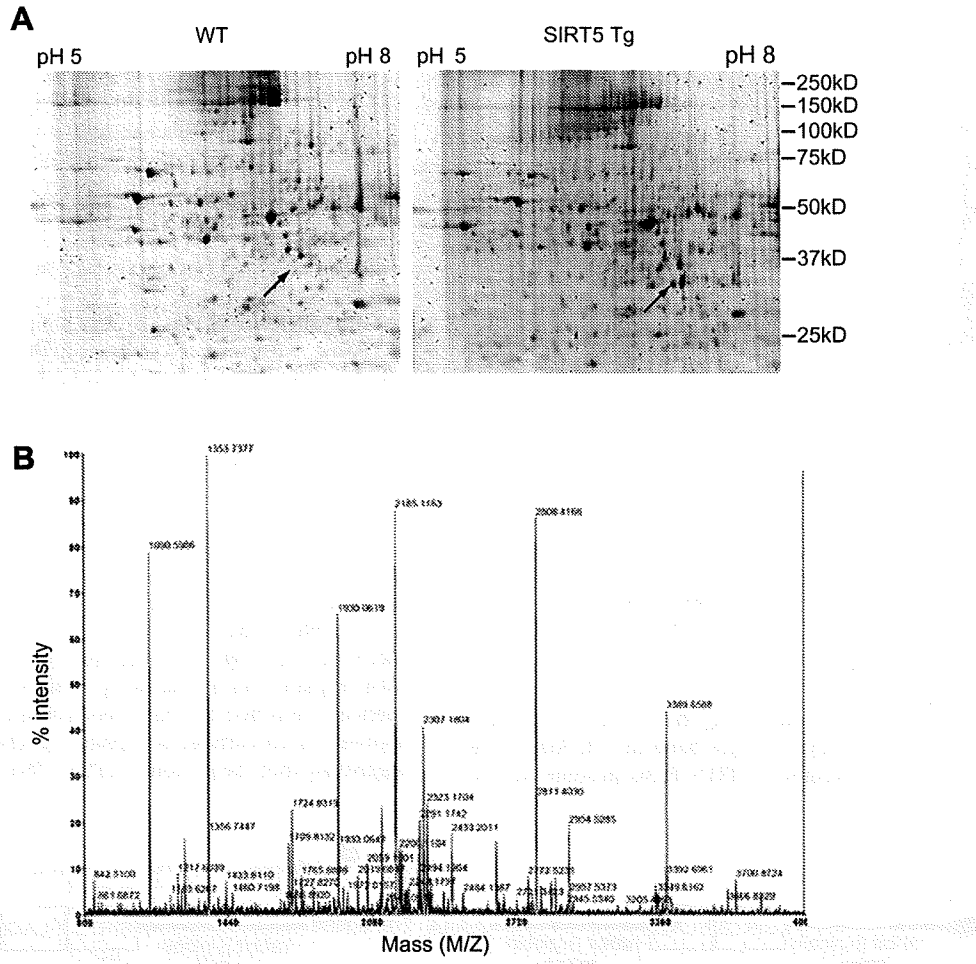

Fig. 3. Identification of the target protein of SIRT5. (A) Two-dimensional electrophoresis of mitochondrial proteins prepared from livers of SIRT5 Tg and wild-type mice. The position of the mitochondrial protein prepared from SIRT5 Tg liver identified by MALDI-TOF-MS is shown by arrow (right panel). The protein is not detected at the corresponding position (indicated by arrow, left panel) in wild-type liver. (B) MALDI-TOF-MS analysis. The mitochondrial protein prepared from SIRT5 Tg liver indicated in (A) was analyzed using MALDI-TOF-MS.

Table 1
Characterization by MALDI-TOF-MS of the target protein of SIRT5.

Measured peptide mass (Da)	Predicted peptide sequence	Start–end
1090.5986	KVPAIYGVDTRM	157–166
1217.6039	KSLGQWLQEEKV	147–156
1353.7377	RGQNQPVLNITNRQ	316–327
1723.8272	KIEFEGQSVDFVDPNKQ	182–196
1930.0619	KEPLFGISTGNIITGLAAGAKS	287–306
2058.1598	RKEPLFGISTGNIITGLAAGAKS	286–306
2184.1154	KGQILTMANPIIGNGGAPDTTARD	90–111
2807.4071	KIEFEGQSVDFVDPNKQNLIAEVSTKD	182–206
2953.5338	KGQILTMANPIIGNGGAPDTTARDELGLNKY	90–118
3662.8010	KMKGYSFGHPSSVAGEVVFNTGLGGYPEALTDPAYKG	55–89

Mass of peptides corresponding to a tryptic digest of CPS1. The corresponding sequence and position (number of amino acid residues) in the sequence are indicated.

expressed predominantly in liver, and catalyzes condensation of ammonia and bicarbonate to carbamoyl phosphate, which is the first step in the urea cycle in liver [15,16].

CPS1 is deacetylated in SIRT5 Tg liver

Since CPS1 is known to be an acetylated protein [26], we investigated deacetylation of CPS1 protein by SIRT5. The mitochondrial protein prepared from livers of SIRT5 Tg and wild-type mice fed *ad libitum* were immunoprecipitated with an anti-acetylated lysine antibody followed by immunoblotting using anti-CPS1 antibody. Acetylated CPS1 protein levels in SIRT5 Tg ($N = 3$) mice were 40% lower than those in wild-type mice ($N = 3$), although total CPS1 expression levels were similar (Fig. 4A). To determine whether SIRT5 protein regulates CPS1 activities, livers of SIRT5 Tg and wild-type mice were homogenized and CPS1 activities were measured. CPS1 activities were significantly increased approximately 2-fold in SIRT5 Tg mice ($N = 5$, $P < 0.01$) compared to those in wild-type mice (Fig. 4B). These results demonstrate that SIRT5 protein deacetylates CPS1 and upregulates its activity in liver.

Urea production is upregulated in SIRT5 Tg hepatocytes

To verify that SIRT5 is involved in the urea cycle by regulating CPS1 activity, production of urea in primary cultured hepatocytes was evaluated. Primary hepatocytes were isolated from SIRT5 Tg and wild-type mice and incubated with ammonia, bicarbonate, and ornithine for 1 h, and the amount of urea synthesized was determined by measuring the urea concentration in the media. Hepatocytes from SIRT5 Tg mice produced more urea than those of wild-type mice (44%, $N = 4$, $P < 0.01$) (Fig. 4C), indicating that urea synthesis is upregulated by overexpression of SIRT5 in liver.

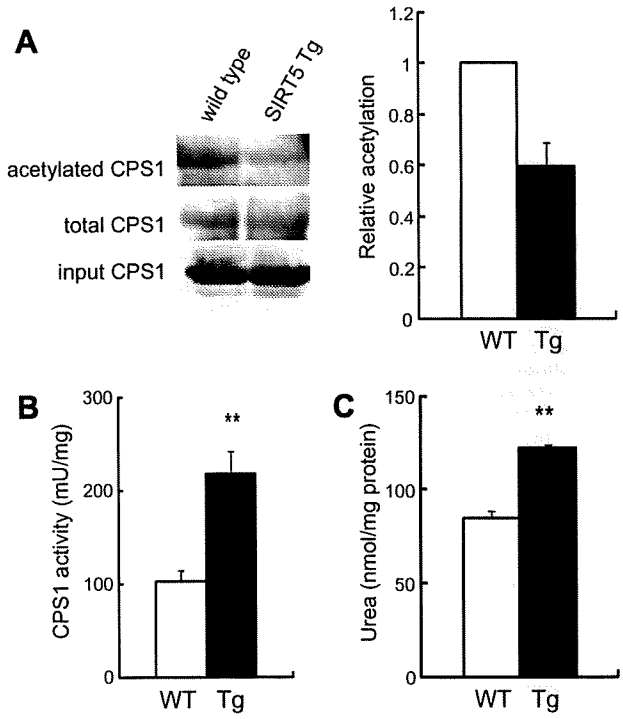

Fig. 4. Deacetylation and activation of CPS1 in livers of SIRT5 Tg mice. (A) CPS1 deacetylation in livers of SIRT5 Tg mice. The mitochondrial protein from livers of SIRT5 Tg and wild-type mice fed *ad libitum* were immunoprecipitated with anti-acetylated lysine antibody (left upper panel) and anti-CPS1 antibody (left middle panel), and immunoblotted with anti-CPS1 antibody. The right panel shows acetylation of CPS1 protein. The ratio of acetylated CPS1 protein of SIRT5 Tg liver to that of wild-type liver was calculated from densitometry of western blots ($N = 3$). (B) Activation of CPS1 activity in SIRT5 Tg liver. Livers of SIRT5 Tg ($N = 5$) and wild-type ($N = 5$) mice fasted for 16 h were homogenized and CPS1 activities were determined as described in Materials and methods. (C) Production of urea in primary cultured hepatocytes. Primary hepatocytes were isolated from SIRT5 Tg ($N = 4$) and wild-type ($N = 4$) mice fasted for 16 h and incubated with $NaHCO_3$ (25 mM), NH_4Cl (10 mM) and ornithine–HCl (5 mM) for 1 h. The amount of urea synthesized was determined by measuring the urea concentration in the media as described in Materials and methods. Values are means ± SEM. $^*P < 0.05$. $^{**}P < 0.01$.

Discussion

In the present study, SIRT5 mRNA levels in liver were found to be increased by fasting. To investigate the function of SIRT5 in liver, we established SIRT5 Tg mice and identified CPS1 as the target protein of SIRT5 by analyses of liver mitochondrial proteins using two-dimensional electrophoresis and MALDI-TOF-MS. We found that CPS1 is deacetylated and that CPS1 activity is significantly increased in the liver of SIRT5 Tg mice. CPS1 is the first and key enzyme of the urea cycle, condensing ammonia with bicarbonate to generate carbamoyl phosphate [15,16]. In hepatocytes from SIRT5 Tg mice, urea synthesis was upregulated compared to that in wild-type mice.

Which residue on CPS1 is deacetylated by SIRT5 is still unclear. The protein that we identified as a target of SIRT5 using two-dimensional electrophoresis and MALDI-TOF-MS was the N-terminal domain of CPS1 (Table. 1), suggesting that the lysine residue of CPS1 deacetylated by SIRT5 is contained in this domain. As Kim et al. reported that CPS1 has nine lysine acetylation sites [26], at least Lys55, Lys119, and/or Lys287 among these lysine residues located in the N-terminal domain might be deacetylated by SIRT5.

During fasting, circulating amino acids, especially alanine, are derived by lysis of muscle proteins, and the amino acids are catalyzed in liver by α-ketoglutarate aminotransferase to generate pyruvate and glutamate. Pyruvate is used in gluconeogenesis to maintain plasma glucose levels, and glutamate is catalyzed by glutamate dehydrogenase to form α-ketoglutarate and ammonia. Ammonia is extremely toxic; the urea cycle converts ammonia to non-toxic urea, which is readily excreted from kidney. It also has been reported that CPS1 activity is increased by fasting or calorie restriction in rodent liver [27,28]. Thus, SIRT5 protein may be involved in detoxification of ammonia during fasting through deacetylation and activation of CPS1.

Recently, Nakagawa et al. reported that CPS1 activity is downregulated in liver of SIRT5 KO mice, which exhibit hyperammonemia by fasting [14]. We show here that CPS1 activity in liver is upregulated in SIRT5 Tg mice during fasting and that urea synthesis is upregulated in SIRT5 Tg hepatocytes, complementing their data.

Suggesting the mechanism of CPS1 activation during fasting, SIRT5 mRNA expression levels in liver were increased by fasting, but protein expression levels were not altered under the same condition in wild-type mice (Supplemental Fig. 1). Nakagawa et al. reported that SIRT5 protein expression levels were not altered, but that NAD levels were elevated by fasting in wild-type mice [14], suggesting that CPS1 is not activated by an increase in SIRT5 protein levels but by activation of SIRT5 through elevation of NAD.

SIRT5 protein is highly expressed in organs other than liver, including kidney, skeletal muscle, and heart (Supplemental Fig. 1), where their functions are yet unknown. Further investigation of the pathophysiological role of SIRT5 is required.

Acknowledgments

This study was supported by Scientific Research Grants from the Ministry of Education, Culture, Sports, Science, and Technology of Japan, from the Ministry of Health, Labor, Welfare, Japan, and by the Kyoto University Global COE Program "Center for Frontier Medicine".

Appendix A. Supplementary data

Supplementary data associated with this article can be found, in the online version, at doi:10.1016/j.bbrc.2010.01.081.

Reference

[1] S. Imai, C.M. Armstrong, M. Kaeberlein, et al., Transcriptional silencing and longevity protein SIR2 is an NAD-dependent histone deacetylase, Nature 403 (2000) 795–800.
[2] M. Kaeberlein, M. McVey, L. Guarente, The SIR2/3/4 complex and SIR2 alone promote longevity in saccharomyces cerevisiae by two different mechanisms, Genes Dev. 13 (1999) 2570–2580.
[3] H.A. Tissenbaum, L. Guarente, Increased dosage of a *sir-2* gene extends lifespan in *Caenorhabditis elegans*, Nature 410 (2001) 227–230.
[4] B. Rogina, S.L. Helfand, SIR2 mediates longevity in the fly through a pathway related to calorie restriction, Proc. Natl. Acad. Sci. USA 101 (2004) 15998–16003.
[5] R.A. Frye, Phylogenetic classification of prokaryotic and eukaryotic SIR2-like proteins, Biochem. Biophys. Res. Commun. 273 (2000) 793–798.
[6] J.T. Rodgers, C. Lerin, W. Haas, S.P. Gygi, et al., Nutrient control of glucose homeostasis through a complex of PGC-1α and SIRT1, Nature 434 (2005) 113–118.
[7] D. Frescas, L. Valent, D. Accili, Nuclear trapping of the forkhead transcription factor FOXO1 via SIRT-dependent deacetylation promotes expression of glucogenetic genes, J. Biol. Chem. 280 (2005) 20589–20595.
[8] Y. Nakamura, M. Ogura, D. Tanaka, et al., Localization of mouse mitochondrial SIRT proteins: shift of SIRT3 to nucleus by co-expression with SIRT5, Biochem. Biophys. Res. Commun. 366 (1) (2008) 174–179.
[9] W.C. Hallows, S. Lee, J.M. Denu, Sirtuins deacetylate and activate mammalian acetyl-CoA synthetases, Proc. Natl. Acad. Sci. USA 103 (2006) 10230–10235.
[10] B. Schwer, J. Bunkenborg, R.O. Verdin, et al., Reversible lysine acetylation controls the activity of the mitochondrial enzyme acetyl-CoA synthetase 2, Proc. Natl Acad. Sci. USA 103 (2005) 10224–10229.
[11] C. Schlicker, M. Gertz, P. Papatheodorou, et al., Substrates and regulation mechanisms for the human mitochondrial sirtuins SIRT3 and SIRT5, J. Mol. Biol. 382 (2008) 790–801.
[12] M.C. Haigis, R. Mostoslavsky, K.M. Haigis, et al., SIRT4 inhibits glutamate dehydrogenase and opposes the effects of calorie restriction in pancreatic beta cells, Cell 126 (2006) 941–954.

[13] B.J. North, B.L. Marshall, M.T. Borra, et al., The human SIR2 ortholog, SIRT2, is an NAD+-dependent tubulin deacetylase, Mol. Cell. 11 (2003) 437–444.
[14] T. Nakagawa, D.J. Lomb, M. Haigis, et al., SIRT5 deacetylates carbamoyl phosphate synthetase 1 and regulates the urea cycle, Cell 137 (2009) 560–570.
[15] M.J. Jackson, A.L. Beaudet, W.E. O'Brien, Mammalian urea cycle enzymes, Annu. Rev. Genet. 20 (1986) 431–464.
[16] J.L. Deignan, S.D. Cederbaum, W.W. Grody, Contrasting features of urea cycle disorders in human patients and knockout mouse models, Mol. Genet. Metab. 93 (2008) 7–14.
[17] J. Miyazaki, K. Araki, E. Yamato, et al., Establishment of a pancreatic beta cell line that retains glucose-inducible insulin secretion: special reference to expression of glucose transporter isoforms, Endocrinology 127 (1990) 126–132.
[18] H. Niwa, K. Yamamua, J. Miyazaki, Efficient selection for high-expression transfectants with a novel eukaryotic vector, Gene 108 (1991) 193–200.
[19] S. Gupta, L.K. Rogers, S.K. Taylor, et al., Inhibition of carbamyl phosphate synthetase-I and glutamine synthetase by hepatotoxic doses of acetaminophen in mice, Toxicol. Appl. Pharmacol. 146 (1997) 317–327.
[20] L.A. Fahien, P.P. Cohen, A kinetic study of carbamyl phosphate synthetase, J. Biol. Chem. 239 (1964) 1925–1934.
[21] M. Hosokawa, B. Thorens, Glucose release from GLUT2-null hepatocytes: characterization of a major and a minor pathway, Am. J. Physiol. Endocrinol. Metab. 282 (2002) E794–801.
[22] D.M. Cyr, S.G. Egan, C.M. Brini, et al., On the mechanism of inhibition of gluconeogenesis and ureagenesis by sodium benzoate, Biochem. Pharmacol. 42 (1991) 645–654.
[23] D. Hunninghake, S. Grisolia, A sensitive and convenient micromethod for estimation of urea, citrulline, and carbamyl derivatives, Anal. Biochem. 16 (1966) 200–205.
[24] W.R. Fearon, The carbamido diacetyl reaction: a test for citrulline, Biochem. J. 33 (1939) 902–907.
[25] S. Nemoto, M.M. Fergusson, T. Finkel, Nutrient availability regulates SIRT1 through a forkhead-dependent pathway, Science 306 (2004) 2105–2108.
[26] S.C. Kim, R. Sprung, Y. Chen, et al., Substrate and functional diversity of lysine acetylation revealed by a proteomics survey, Mol. Cell. 23 (2006) 607–618.
[27] M. Gomez, A. Jorda, J. Cabo, et al., Effect of starvation on the N-acetylglutamate system of rat liver, FEBS. Lett. 156 (1983) 119–122.
[28] J.B. Tillman, J.M. Dhahbi, P.L. Mote, et al., Dietary calorie restriction in mice induces carbamyl phosphate synthetase I gene transcription tissue specifically, J. Biol. Chem. 271 (1996) 3500–3506.

Heterozygous variants of multidrug and toxin extrusions (MATE1 and MATE2-K) have little influence on the disposition of metformin in diabetic patients

Kana Toyama[a], Atsushi Yonezawa[a], Masahiro Tsuda[a], Satohiro Masuda[a], Ikuko Yano[a], Tomohiro Terada[a], Riyo Osawa[a], Toshiya Katsura[a], Masaya Hosokawa[b], Shimpei Fujimoto[b], Nobuya Inagaki[b] and Ken-Ichi Inui[a]

Multidrug and toxin extrusions (MATE1/SLC47A1 and MATE2-K/SLC47A2) play important roles in the renal excretion of metformin. We have previously identified the nonsynonymous *MATE* variants with functional defects at low allelic frequencies. The purpose of this study was to evaluate the effects of heterozygous *MATE* variants on the disposition of metformin in mice and humans. Pharmacokinetic parameters of metformin in *Mate1*(±) heterozygous mice were comparable with those in *Mate1*(+/+) wild-type mice. Among 48 Japanese diabetic patients, seven patients carried heterozygous *MATE* variant and no patient carried homozygous *MATE* variant. There was no significant difference in oral clearance of metformin with or without heterozygous *MATE* variants. In addition, creatinine clearance, but not heterozygous *MATE* variants, significantly improved the model fit of metformin clearance by statistical analysis using the nonlinear mixed-effects modeling program. In conclusion, heterozygous *MATE* variants could not influence the disposition of metformin in diabetic patients. *Pharmacogenetics and Genomics* 20:135–138 © 2010 Wolters Kluwer Health | Lippincott Williams & Wilkins.

Pharmacogenetics and Genomics 2010, 20:135–138

Keywords: creatinine clearance, H^+/organic cation antiporter, metformin, organic cation transporter, pharmacokinetics

[a]Department of Pharmacy, Faculty of Medicine, Kyoto University Hospital and [b]Department of Diabetes and Clinical Nutrition, Graduate School of Medicine, Kyoto University, Sakyo-ku, Kyoto, Japan

Correspondence to Professor Ken-ichi Inui, PhD, Department of Pharmacy, Kyoto University Hospital, Sakyo-ku, Kyoto 606-8507, Japan
Tel: +81 75 751 3577; fax: +81 75 751 4207;
e-mail: inui@kuhp.kyoto-u.ac.jp

Received 17 September 2009 Accepted 16 November 2009

Metformin is widely used for the treatment of hyperglycemia in patients with noninsulin-dependent diabetes mellitus. The major pharmacological action of metformin involves the suppression of gluconeogenesis in the liver. Lactic acidosis is a rare but serious adverse effect of metformin, which occurs predominantly in patients with renal insufficiency. Clinical pharmacokinetic studies revealed that metformin is mainly excreted into urine in an unchanged form without hepatic metabolism, and that the renal clearance of metformin is approximately five times higher than creatinine clearance (Ccr) [1], suggesting that renal tubular secretion is a major route of metformin elimination. In human proximal tubules, multidrug and toxin extrusion 1 (MATE1/SLC47A1) and a kidney-specific isoform MATE2-K/SLC47A2 are localized at the brush-border membranes, which were characterized as H^+/organic cation antiporters [2]. In rodents, Mate1, but not Mate2, is expressed in the kidney [2]. Metformin is a substrate for MATE1 and MATE2-K, as well as organic cation transporter 2 (OCT2/SLC22A2), which is localized at the basolateral membranes of the kidney [2,3]. The functional significance of MATE in the kidney was previously shown using *Mate1* knockout mice [4]. On the basis of these backgrounds and findings, MATE1 and MATE2-K could play key roles in metformin tubular secretion in humans.

Genetic variants in *MATE* genes are likely to be one of the factors for interindividual variability in metformin pharmacokinetics and pharmacodynamics. Recently, we and another group identified nonsynonymous single nucleotide polymorphisms (SNPs) in coding region of *MATE* genes, some of which reduced the transport activity [5,6]. In addition, Becker *et al.* [7] reported that rs2289669G > A SNP in the *MATE1* gene was associated with the glucose-lowering effect, but metformin pharmacokinetics was not evaluated. Tzvetkov *et al.* [8] demonstrated that there was no relationship between the same SNP and metformin pharmacokinetics. However, rs2289669G > A SNP in the *MATE1* gene was located in noncoding intron region and there was no information about the effect of this non-coding SNP on the transport activity. Therefore, it is not clear whether the functional reduced nonsynonymous *MATE* variants alter metformin disposition. The allelic frequencies of all *MATE* variants were quite low, in the range of 0.6–2.4% [5,6]. Homozygous variants with functional loss of transport activity decrease drug elimination in most

Supplemental digital content is available for this article. Direct URL citations appear in the printed text and are provided in the HTML and PDF versions of this article on the journal's Website (*www.pharmacogeneticsandgenomics.com*).

1744-6872 © 2010 Wolters Kluwer Health | Lippincott Williams & Wilkins

DOI: 10.1097/FPC.0b013e328335639f

cases. The effect of heterozygous variants, in contrast, depends on the transporters and the drugs. In the breast cancer resistance protein (*BCRP/ABCG2*) gene, heterozygous Q141K variant caused elevated oral bioavailability of its substrate [9]. These results suggested that information about the influence of heterozygous as well as homozygous *MATE* variants on metformin pharmacokinetics is required for its safe use in clinical situations. In this study, therefore, we focused on the effect of heterozygous nonsynonymous *MATE* variants on metformin disposition in diabetic patients.

Using *Mate1*(+/+) wild-type, *Mate1*(±) heterozygous and *Mate1*(−/−) homozygous mice, we first examined the pharmacokinetics of metformin (Supplemental methods, Supplemental digital content 1 *http://links.lww.com/FPC/A82*). High plasma concentration and low urinary excretion of metformin were observed in *Mate1*(−/−) mice compared with *Mate1*(+/+) mice, whereas there was no difference between *Mate1*(±) and *Mate1*(+/+) mice (Fig. 1a and b). In addition, several pharmacokinetic parameters in *Mate1*(±) mice were comparable with those in *Mate1*(+/+) mice (Supplemental Table 1, Supplemental digital content 2 *http://links.lww.com/FPC/A83*). Mate1 protein expression levels in these three genotype mice are shown in Fig. 1c. The transport of metformin by HEK293 cells expressing mouse Mate1, mouse Oct1 or mouse Oct2 was confirmed (Supplemental Fig. 1, Supplemental digital content 3 *http://links.lww.com/FPC/A84*). Based on these results, we hypothesized that the heterozygous *MATE* variants do not influence on the metformin clearance in humans as well as in mice.

To address the species difference in *MATE* genes, pharmacokinetic evaluation was also carried out in humans. Forty-eight Japanese patients with diabetes mellitus were enrolled into this study. Blood samples were obtained at 0, 4, and 9 h after metformin administration, followed by the determination of plasma concentrations and genotype for *MATE1*, *MATE2-K*, and *OCT2* genes (Supplemental methods, Supplemental digital content 1 *http://links.lww.com/FPC/A82*). The oral clearance (CL/F) of metformin in diabetic patients was estimated by the empirical Bayesian method with the nonlinear mixed-effects modeling program NONMEM using a basic model: CL/F=θ1. Two MATE1-G64D variant carriers, two MATE1-L125F variant carriers, and one MATE1-D328A variant carrier were found in this study. In the *MATE2-K* gene, the G211V variant was found in two patients. All *MATE* variant carriers were heterozygotes and included in the *MATE*-heterozygous variant group. The plasma concentration–time profile after an oral administration of metformin in *MATE*-heterozygous variant group was similar to that in *MATE*-reference group (Supplemental Fig. 2, Supplemental digital content 4 *http://links.lww.com/FPC/A85*). Patient

Fig. 1

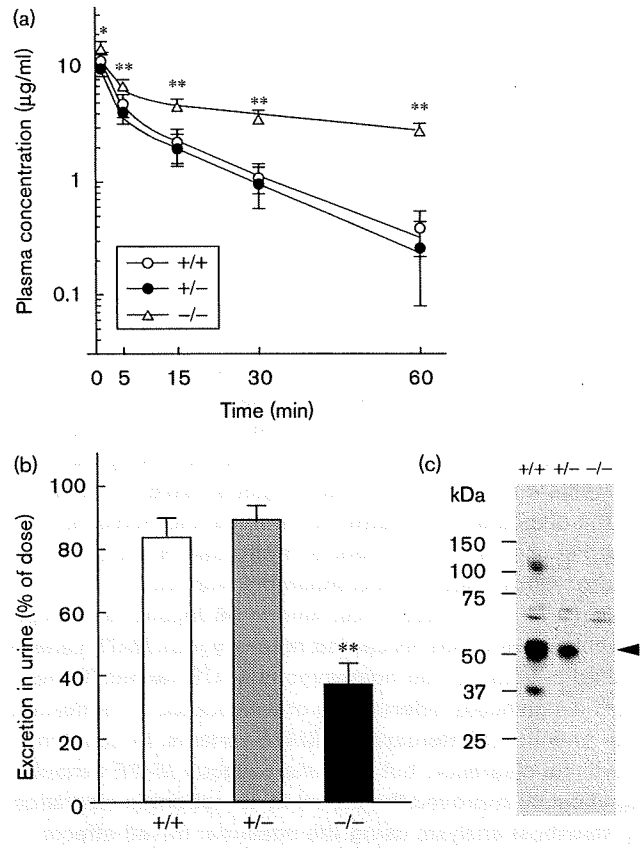

Metformin pharmacokinetic studies of *Mate1*(+/+), *Mate1*(±), and *Mate1*(−/−) mice. (a) Plasma concentration–time profiles were obtained after the intravenous administration of metformin to *Mate1* (+/+) (open circles), *Mate1*(±) (closed circles), and *Mate1*(−/−) (open triangles) mice. (b) Urinary excretion of metformin in *Mate1* (+/+) (open column), *Mate1*(±) (gray column), and *Mate1*(−/−) (closed column) mice were calculated using urine samples collected for 60 min after the drug administration. Each column represents the mean ± SD for six to eight mice. **P*<0.05, ***P*<0.01, significantly different from *Mate1*(+/+) mice. (c) Western blot analysis of Mate1 in renal brush-border membrane fractions was carried out. The arrowhead indicates the position of mouse Mate1.

characteristics were similar between the two groups. There was no statistically significant difference in metformin CL/F between the *MATE*-heterozygous variant group and the *MATE*-reference group (Table 1). All of 11 *OCT2* variant carriers were also heterozygotes. Only one patient carried both MATE1-G64D and OCT2-A270S variants. The CL/F values of the *MATE*-variant group, the *OCT2*-variant group and both the *MATE*-variant and *OCT2*-variant group were comparable with those of the reference group (Supplemental Table 2, Supplemental digital content 5 *http://links.lww.com/FPC/A86*).

To determine the most important factor contributing to interindividual variability in metformin CL/F, we examined the relationship between CL/F and patient characteristics, such as age, sex, renal function, and

Table 1 Patient characteristics and effects of heterozygous *MATE* variants on metformin oral clearance in 48 Japanese patients with diabetes mellitus

	MATE reference	MATE-heterozygous variant[a]
Patients	41	7
Sex (male/female)	17/24	1/6
Age (years)	62±10	67±8
BMI (kg/m^2)	27±4	25±3
Metformin CL/F (ml/min)	603±137	658±115
Ccr (ml/min)	98±34	83±37
eGFR (ml/min)	71±23	71±21

Ccr, 24-h creatinine clearance; CL/F, oral clearance of metformin; eGFR, estimated glomerular filtration rate; MATE, multidrug and toxin extrusion.
[a]*MATE*-heterozygous variant includes MATE1-G64D (n=2), MATE1-L125F (n=2), MATE1-D328A (n=1), MATE2-K-G211V (n=2). No patient carried other *MATE* variants; MATE1-V10L, MATE1-A310V, MATE1-V338I, MATE1-N474S, MATE1-V480M, MATE1-C497S, MATE1-Q519H, and MATE2-K-K64N. Data are expressed as mean±SD. There was no statistically significant difference between two groups.

transporter genetic variations. Regression analysis showed that metformin CL/F was positively correlated with both Ccr and estimated glomerular filtration rate (eGFR) (Supplemental Fig. 3, Supplemental digital content 6 *http://links.lww.com/FPC/A87*). In NONMEM analysis, model fit was significantly improved for the models using the individual Ccr or eGFR compared with the basic model (CL/F=θ1). However, there was no improvement in the models with age, sex or genetic variants of the *MATE* or *OCT2* gene. A negative of twice the log likelihood difference (−2LLD) value was higher in the model using Ccr than that using eGFR (Supplemental Table 3, Supplemental digital content 7 *http://links.lww.com/FPC/A88*). The incorporation of Ccr into the basic model explained part of the interindividual variability in CL/F, with its value decreasing from 26.1 to 19.6%.

Interindividual variability in MATE activity is likely to affect the pharmacokinetics of metformin. Examination with *Mate1* knockout mice strongly suggested the pharmacokinetic alternation in humans with the functional defect homozygous variants [4]. However, homozygous variants in *MATE1* and *MATE2-K* genes were reported to be quite rare [5,6]. Therefore, we examined the pharmacokinetic significance of the heterozygous *MATE* variants to clarify whether we should pay attention to these genotypes in the clinical situations. As expected from the animal data, the heterozygous *MATE* variants did not affect the disposition of metformin in humans (Fig. 1 and Table 1). The rate-limiting step in the renal secretion of metformin is either the renal blood flow, the tubular uptake across the basolateral membranes or efflux into the lumen at the brush-border membranes. In this study, heterozygous *MATE* variants did not affect metformin clearance, although MATE1 and MATE2-K were important for metformin secretion [2,3]. Likewise, heterozygous *OCT2* variant did not affect metformin clearance in diabetic patients, even though the pharmacokinetic effect of *OCT2* variant is still controversial [3,8,10]. The renal clearance of metformin was reported to be in the range of 335–615 ml/min in humans [1], which is comparable with renal plasma flow. These results suggested that renal blood flow is a rate-limiting factor for metformin secretion. Therefore, heterozygous *MATE* variants possibly show only a minor portion in the interindividual variation of metformin pharmacokinetics in clinical situations.

For determination of the most important factor contributing to metformin disposition among age, sex, renal function, and heterozygous variations of *MATE* and *OCT2* genes, NONMEM analysis was carried out. Consistent with previous reports [1,8], we showed that Ccr is a significant predictor of metformin clearance. Although Ccr is used clinically as a marker of GFR, Ccr is known to overestimate GFR because of the creatinine tubular secretion. Previously, we showed that creatinine is a substrate for OCT2, MATE1, and MATE2-K [2]. These reports suggested that creatinine as well as metformin is excreted into the urine by tubular secretion through organic cation transport systems in addition to glomerular filtration. Comparable with these findings, metformin CL/F had a higher correlation with Ccr than with eGFR. Therefore, Ccr is the most clinical reliable indicator of metformin disposition.

In conclusion, it was shown that heterozygous *MATE* variants as well as heterozygous *OCT2* variants do not affect metformin disposition in diabetic patients. Moreover, it was revealed that Ccr is the most important factor to predict metformin disposition in the clinical use. On account of the low allelic frequency, further studies are needed with much more patients to determine the effect of homozygous *MATE* variants on metformin disposition in clinical situations.

Acknowledgements

The authors are grateful to all the medical staff of Department of Diabetes and Clinical Nutrition, Graduate School of Medicine, Kyoto University, especially to Dr Chizumi Yamada, Dr Kazuyo Fujita, Dr Akio Obara, Dr Norio Harada, Dr Kazutaka Nagai, and Dr Shiho Takahara for excellent help. This study was supported in part by a grant-in-aid for Scientific Research (KAKENHI) from the Ministry of Education, Science, Culture, and Sports of Japan. M. Tsuda is a Research Fellow of the Japan Society for the Promotion of Science.

References

1 Scheen AJ. Clinical pharmacokinetics of metformin. *Clin Pharmacokinet* 1996; **30**:359–371.
2 Terada T, Inui K. Physiological and pharmacokinetic roles of H$^+$/organic cation antiporters (MATE/SLC47A). *Biochem Pharmacol* 2008; **75**:1689–1696.
3 Takane H, Shikata E, Otsubo K, Higuchi S, Ieiri I. Polymorphism in human organic cation transporters and metformin action. *Pharmacogenomics* 2008; **9**:415–422.

4 Tsuda M, Terada T, Mizuno T, Katsura T, Shimakura J, Inui K. Targeted disruption of the multidrug and toxin extrusion 1 (Mate1) gene in mice reduces renal secretion of metformin. *Mol Pharmacol* 2009; **75**:1280–1286.
5 Kajiwara M, Terada T, Ogasawara K, Iwano J, Katsura T, Fukatsu A, *et al.* Identification of multidrug and toxin extrusion (MATE1 and MATE2-K) variants with complete loss of transport activity. *J Hum Genet* 2009; **54**:40–46.
6 Chen Y, Teranishi K, Li S, Yee SW, Hesselson S, Stryke D, *et al.* Genetic variants in multidrug and toxic compound extrusion-1, hMATE1, alter transport function. *Pharmacogenomics J* 2009; **9**:127–136.
7 Becker MSL, Visser LE, van Schaik RHN, Hofman A, Uitterlinden AG, Stricker BHC. Genetic variation in the multidrug and toxin extrusion 1 transporter protein influences the glucose-lowering effect of metformin in patients with diabetes: a preliminary study. *Diabetes* 2009; **58**:745–749.
8 Tzvetkov MV, Vormfelde SV, Balen D, Meineke I, Schmidt T, Sehrt D, *et al.* The effects of genetic polymorphisms in the organic cation transporters OCT1, OCT2, and OCT3 on the renal clearance of metformin. *Clin Pharmacol Ther* 2009; **86**:299–306.
9 Sparreboom A, Gelderblom H, Marsh S, Ahluwalia R, Obach R, Principe P, *et al.* Diflomotecan pharmacokinetics in relation to ABCG2 421C>A genotype. *Clin Pharmacol Ther* 2004; **76**:38–44.
10 Chen Y, Li S, Brown C, Cheatham S, Castro RA, Leabman MK, *et al.* Effect of genetic variation in the organic cation transporter 2 on the renal elimination of metformin. *Pharmacogenet Genomics* 2009; **19**:497–504.

Rapamycin impairs metabolism-secretion coupling in rat pancreatic islets by suppressing carbohydrate metabolism

Makiko Shimodahira, Shimpei Fujimoto, Eri Mukai, Yasuhiko Nakamura, Yuichi Nishi, Mayumi Sasaki, Yuichi Sato, Hiroki Sato, Masaya Hosokawa, Kazuaki Nagashima, Yutaka Seino[1] and **Nobuya Inagaki**

Department of Diabetes and Clinical Nutrition, Graduate School of Medicine, Kyoto University, 54 Shogoin Kawahara-cho, Sakyo-ku, Kyoto 606-8507, Japan
[1]Kansai Electric Power Hospital, Osaka 553-0003, Japan
(Correspondence should be addressed to S Fujimoto; Email: fujimoto@metab.kuhp.kyoto-u.ac.jp)

Abstract

Rapamycin, an immunosuppressant used in human transplantation, impairs β-cell function, but the mechanism is unclear. Chronic (24 h) exposure to rapamycin concentration dependently suppressed 16·7 mM glucose-induced insulin release from islets (1·65±0·06, 30 nM rapamycin versus 2·35±0·11 ng/islet per 30 min, control, $n=30$, $P<0·01$) without affecting insulin and DNA contents. Rapamycin also decreased α-ketoisocaproate-induced insulin release, suggesting reduced mitochondrial carbohydrate metabolism. ATP content in the presence of 16·7 mM glucose was significantly reduced in rapamycin-treated islets (13·42 ±0·47, rapamycin versus 16·04±0·46 pmol/islet, control, $n=30$, $P<0·01$). Glucose oxidation, which indicates the velocity of metabolism in the Krebs cycle, was decreased by rapamycin in the presence of 16·7 mM glucose (30·1±2·7, rapamycin versus 42·2±3·3 pmol/islet per 90 min, control, $n=9$, $P<0·01$). Immunoblotting revealed that the expression of complex I, III, IV, and V was not affected by rapamycin. Mitochondrial ATP production indicated that the respiratory chain downstream of complex II was not affected, but that carbohydrate metabolism in the Krebs cycle was reduced by rapamycin. Analysis of enzymes in the Krebs cycle revealed that activity of α-ketoglutarate dehydrogenase (KGDH), which catalyzes one of the slowest reactions in the Krebs cycle, was reduced by rapamycin (10·08±0·82, rapamycin versus 13·82 ±0·84 nmol/mg mitochondrial protein per min, control, $n=5$, $P<0·01$). Considered together, these findings indicate that rapamycin suppresses high glucose-induced insulin secretion from pancreatic islets by reducing mitochondrial ATP production through suppression of carbohydrate metabolism in the Krebs cycle, together with reduced KGDH activity.
Journal of Endocrinology (2010) **204,** 37–46

Introduction

Rapamycin, an immunosuppressant used in human organ and tissue transplantation, exhibits a different mechanism of action from that of cyclosporine, tacrolimus, and corticosteroids. The agent is a macrolide that prevents T-cell activation through its inhibitory effect on serine/threonine kinase, the mechanistic target of rapamycin (MTOR). The insulin- and nutrient-signaling pathway through MTOR plays an important role in initiation of protein translation, a critical event in enhanced protein synthesis that leads to increased cell cycle progression and proliferation (McDaniel *et al.* 2002).

Brittle type 1 diabetes has been successfully treated by human islet transplantation using the Edmonton protocol, which includes use of rapamycin as an immunosuppressant (Shapiro *et al.* 2000). Some studies suggest rapamycin may be diabetogenic (Lu *et al.* 1994, Teutonico *et al.* 2005), and the effects of rapamycin on glucose homeostasis have been investigated. In skeletal muscle cells, long-term exposure to rapamycin decreases insulin-dependent uptake of glucose and glycogen synthesis and increases fatty acid oxidation (Sipula *et al.* 2006). Rapamycin also decreases insulin-mediated glucose uptake and insulin signaling in adipocytes (Taha *et al.* 1999, Cho *et al.* 2004). Interestingly, rapamycin both prevents β-cell mass expansion and impairs β-cell function (Bell *et al.* 2003, Zhang *et al.* 2006, Fraenkel *et al.* 2008).

In pancreatic β-cells, intracellular glucose metabolism regulates exocytosis of insulin granules according to metabolism-secretion coupling in which glucose-induced mitochondrial ATP production plays an essential role (Maechler & Wollheim 2001). Since depletion of mitochondrial DNA abolishes the glucose-induced ATP elevation, mitochondria clearly are a major source of ATP production in pancreatic β-cells (Kennedy *et al.* 1998, Tsuruzoe *et al.* 1998). Glucose-induced insulin secretion from β-cells is often impaired due to reduced glucose-induced ATP elevation by exposure to high concentrations of fuels including glucose, free fatty acids, and ketone body, and by administration of diabetogenic pharmacological agents (Fujimoto *et al.* 2007). Thus, reduced mitochondrial ATP production plays an important role in impaired glucose-induced insulin secretion.

Journal of Endocrinology (2010) **204,** 37–46
0022-0795/10/0204-037
DOI: 10.1677/JOE-09-0216
Online version via http://www.endocrinology-journals.org

Recently, several reports have shown that inhibition of MTOR by rapamycin decreases mitochondrial oxidative function using various materials including kidney mitochondria (Simon *et al.* 2003), Jurkat cells (Schieke *et al.* 2006), and skeletal tissue and cells (Cunningham *et al.* 2007). We investigated the effects of chronic exposure to rapamycin on metabolism-secretion coupling, especially on glucose metabolism in mitochondria, in pancreatic β-cells.

Materials and Methods

Materials

Rapamycin was purchased from Calbiochem (La Jolla, CA, USA). Disodium succinate, rotenone, pyruvate potassium, malate, and tetramethyl-*p*-phenyldiamine (TMPD) were purchased from Nacalai (Kyoto, Japan). Mouse monoclonal antibody to the subunits of the mitochondrial respiratory chain complex was obtained from Invitrogen. [5-^{3}H]-glucose, [U-^{14}C]-glucose, and anti-mouse IgG HRP-conjugated secondary antibody were obtained from GE Healthcare (Buckinghamshire, UK). Acetyl-CoA was obtained from Wako (Osaka, Japan). Luciferin–luciferase was obtained from Promega. All other reagents were obtained from Sigma Chemicals.

Animals

Male Wistar rats were obtained from Shimizu Co. (Kyoto, Japan). The animals were fed standard laboratory chow *ad libitum* and allowed free access to water in an air-conditioned room with a 12 h light:12 h darkness cycle until the experiments. All experiments were carried out with rats aged 8–11 weeks. The animals were maintained and used in accordance with the Guidelines for Animal Experiments of Kyoto University.

Islet isolation and culture

Islets of Langerhans were isolated from Wistar rats by collagenase digestion as previously described (Fujimoto *et al.* 1998). Isolated islets were cultured for 24 h in RPMI 1640 medium containing 10% FCS, 100 U/ml penicillin, 100 μg/ml streptomycin, and 5·5 mM glucose with or without rapamycin, at 37 °C in humidified air containing 5% CO_2.

Measurement of insulin release from isolated rat pancreatic islets, insulin content, and DNA content

Insulin release from intact islets was monitored using batch incubation as previously described (Fujimoto *et al.* 1998) using Krebs-Ringer bicarbonate buffer (KRBB) supplemented with 0·2% BSA (fraction V) and 10 mM HEPES adjusted to pH 7·4 (KRBB medium). After cultured islets were preincubated at 37 °C for 30 min in KRBB medium supplemented with 2·8 mM glucose, groups of five islets were batch incubated for 30 min in 0·7 ml KRBB medium containing 2·8 and 16·7 mM glucose with or without 100 μM α-tocopherol plus 200 μM ascorbate, or containing 2·8 and 16·7 mM α-ketoisocaproate (KIC). Before addition to KRBB medium, α-tocopherol was dissolved in ethanol at 1000-fold concentration. The same amount of ethanol was added to the control solution. At the end of the incubation period, the islets were pelleted by centrifugation, and aliquots of the buffer were sampled to determine the amount of immunoreactive insulin by RIA. After an aliquot of incubation medium for insulin release assay was taken, the islets remaining were lysed to determine insulin and DNA contents as previously described (Fujimoto *et al.* 2000).

Measurement of ATP content

ATP contents were determined as previously described (Kominato *et al.* 2008). Briefly, after groups of cultured islets were preincubated at 2·8 mM glucose for 30 min, groups of ten islets were incubated in tubes containing 0·5 ml KRBB medium supplemented with 2·8 or 16·7 mM glucose with or without 100 μM α-tocopherol plus 200 μM ascorbate at 37 °C for 30 min. Incubation was stopped by the addition of 0·1 ml of 2 M $HClO_4$. The contents of tubes were immediately mixed with vortex and sonicated in ice-cold water. The tubes were then centrifuged, and a fraction (0·4 ml) of the supernatant was mixed with 0·1 ml of 2 M HEPES and 0·1 ml of 1 M Na_2CO_3. The ATP concentration was measured by adding 0·2 ml luciferin–luciferase solution to a fraction sample (0·1 ml) in a bioluminometer (Luminometer Model 20e, Turner Designs, Sunnyvale, CA, USA). To draw a standard curve, blanks and ATP standards were run through the entire procedure including the extraction steps.

Measurement of glucose utilization and oxidation

Glucose utilization and oxidation were measured using the previously described method (Nabe *et al.* 2006). Briefly, cultured islets were preincubated in KRBB medium with 2·8 mM glucose at 37 °C for 30 min. For glucose utilization measurements, tubes containing 25 islets in 150 μl KRBB medium containing 2·8 or 16·7 mM glucose and 1·5 μCi [5-^{3}H] glucose were placed into glass vials containing 0·5 ml water. The capped vials were incubated at 37 °C for 90 min. After incubation was stopped by adding 50 μl of 1 M HCl into the incubation medium of the tubes without opening the caps, the capped vials were incubated overnight at 34 °C to allow $^{3}H_2O$ in the tubes to equilibrate with the water in the vial. Each tube was removed, and the disintegrations per minute of $^{3}H_2O$ in the water were counted. For oxidation measurements, procedures were the same as those for utilization measurements, except for the use of [U-^{14}C] glucose (0·5 μCi/tube) in place of [5-^{3}H] glucose and the use of 0·5 ml hydroxide of hyamine 10-X (Packard, Meriden, CT, USA) in place of 0·5 ml water.

Measurement of glucokinase activity

Glucokinase activity was measured by a fluorometric assay as previously described (Radu *et al.* 2005). Briefly, after cultured islets were preincubated with KRBB medium with 2·8 mM glucose, 100 islets were homogenized and the supernatants (islet extracts) were obtained from the homogenates by centrifugation. The glucose phosphorylation rate was estimated as the increase in NADH through the following reaction: glucose-6-phosphate + NAD^+ → 6-phosphoglucono-δ-lactone + NADH by NAD^+-dependent glucose-6-phosphate dehydrogenase (G6PDH). The enzyme reaction was performed using islet extracts in a solution containing NAD^+ and G6PDH supplemented with two concentrations (50 and 0·5 mM) of glucose at 37 °C for 1 h. NADH concentration was measured by fluorometry (Shimazu RF-5000, Kyoto, Japan). Glucokinase activity was determined by subtracting hexokinase activity measured at 0·5 mM glucose from the activity measured at 50 mM glucose.

Measurement of mitochondrial ATP production

Measurement of ATP production from mitochondrial fraction was performed as previously described (Takehiro *et al.* 2005). Briefly, to measure ATP production by oxidative phosphorylation, the reaction was started by adding mitochondrial suspension to prewarmed solution (37 °C) supplemented with the mitochondrial substrates, 50 μM ADP, and 1 μM diadenosine pentaphosphate (DAPP). DAPP is a specific inhibitor of adenylate kinase used to measure ATP production by oxidative phosphorylation exclusively. To normalize the mass of the intact mitochondria obtained, ATP production by adenylate kinase, one of the mitochondrial intermembrane kinases, was measured in the presence of ADP but without mitochondrial substrates or DAPP in parallel incubations. After reaction was stopped, the ATP concentration in the solutions was measured by adding luciferin–luciferase solution with a bioluminometer. ATP production was determined as the ratio of ATP production by oxidative phosphorylation to that by adenylate kinase.

Western blotting of mitochondrial respiratory chain complexes

After washing with ice-cold PBS, the cultured islets were solubilized in ice-cold lysis buffer (10 mM Tris (pH 7·2), 100 mM NaCl, 1 mM EDTA, 1% Nonidet P-40, and 0·5% sodium deoxycholate) containing protease inhibitor cocktail (Complete; Roche) with sonication (5 s pulse, five times). Protein content of the supernatant was measured and adjusted by Bradford method. The supernatant was dissolved in the same amount of SDS-PAGE sample buffer containing 100 mM Tris–HCl (pH 6·80), 4% SDS, 12% 2-mercaptoethanol, 20% glycerol, and 1% bromophenol blue and boiled for 5 min at 95 °C. The samples were subjected to electrophoresis on 12% SDS–polyacrylamide gels and transferred onto nitrocellulose membrane (Schleicher & Schuell, Keene, NH, USA). After blocking with TBS containing 0·1% Tween 20 and 5% skimmed milk (blocking buffer) for 1 h at 4 °C, blotted membranes were incubated overnight at 4 °C with mouse monoclonal anti-complex I (39 kDa subunit), anti-complex III (core II), anti-complex IV (subunit I), or anti-complex V (subunit α) of mitochondrial respiratory chain antibody at 1:1000 dilution in blocking buffer, and subsequently with anti-mouse IgG HRP-conjugated secondary antibody diluted 1:5000 at room temperature for 1 h prior to detection using ECL (GE Healthcare). In the same membrane, the process was repeated for β-actin at 1:5000 dilution of the antibody. Band intensities were quantified with Multi Gauge software (Fujifilm, Tokyo, Japan).

Measurement of activities of enzymes in Krebs cycle

Mitochondrial fraction obtained as described above was sonicated in ice-cold solution containing (mM) 180 KCl, 5 morpholinepropanesulfonic acid, and 2 EDTA adjusted to pH 7·40 and then diluted to each reaction mixture. Enzyme activities including NAD^+-linked isocitrate dehydrogenase (NAD-ICDH), aconitase, α-ketoglutarate dehydrogenase (KGDH), and malate dehydrogenase (MDH) were measured as previously described (Nulton-Persson & Szweda 2001). NAD-ICDH activities were measured as the rate of NAD^+ reduction in solution A containing (mM) 25 KH_2PO_4, 0·5 EDTA, and 0·01% Triton X-100 adjusted to pH 7·25 supplemented with 2·5 mM isocitrate, 40 μM rotenone, 5 mM $MgCl_2$, and 1 mM NAD^+. Aconitase activities were measured as the rate of $NADP^+$ reduction in solution A with 5 mM citrate, 0·6 mM $MgCl_2$, 1·0 U/ml NADP-ICDH, and 0·2 mM $NADP^+$. KGDH activities were measured as the rate of NAD^+ reduction in solution A with 2·5 mM α-ketoglutarate, 40 μM rotenone, 5·0 mM $MgCl_2$, 1 mM NAD^+, 0·1 mM CoA, and 0·2 mM thymine pyrophosphate (TPP). MDH activities were measured as the rate of NAD^+ reduction in solution A with 2·5 mM malate, 40 μM rotenone, 5 mM $MgCl_2$, 10 mM NAD^+, 0·3 mM acetyl-CoA, and 1 U/ml citrate synthase. Enzyme activities of pyruvate dehydrogenase (PDH) were measured as total PDH complex activity (Schwab *et al.* 2005) as the rate of *p*-iodonitrotetrazolium violet (INT) reduction in a reaction mixture containing 5 mM L-carnitine, 1·0 mM $MgCl_2$, 2·5 mM NAD^+, 0·1 mM CoA, 5 mM pyruvate, 0·2 mM TPP, 0·1% Triton X-100, 1 g/l BSA, 0·6 mM INT, and 6·5 mM phenazine methosulfate. All enzyme assays were performed at 25 °C.

Statistical analysis

The data are expressed as the mean ± S.E.M. Statistical significance was calculated by unpaired Student's *t*-test. $P<0·05$ was considered significant.

Results

Effect of chronic exposure to rapamycin on glucose-induced insulin release, insulin content, and DNA content in islets

Chronic (24 h) exposure to rapamycin (10, 30, and 100 nM) concentration dependently suppressed 16·7 mM glucose-induced insulin release (1·94±0·09, 10 nM; 1·65±0·06, 30 nM; 1·50±0·06, 100 nM rapamycin versus 2·35 ±0·11 ng/islet per 30 min, control, $n=30$, $P<0·01$ respectively) but did not affect basal insulin release in the presence of 2·8 mM glucose (Fig. 1A). Insulin secretion divided by insulin content also demonstrates that rapamycin suppresses glucose-induced insulin secretion (Fig. 1A). Insulin and DNA contents were not affected by 24-h exposure to 10, 30, and 100 nM rapamycin (Table 1), indicating that these concentrations of rapamycin do not reduce islet β-cell mass. Reactive oxygen species (ROS) scavengers did not affect suppressed glucose-induced insulin secretion by rapamycin (1·60±0·10, 30 nM rapamycin versus 1·69±0·10 ng/islet per 30 min, 30 nM rapamycin with α-tocopherol plus ascorbate, $n=10$, not significant).

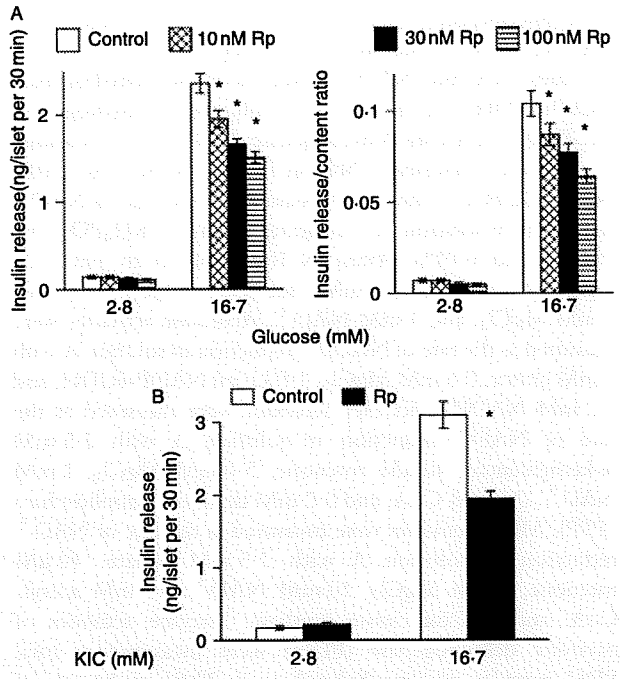

Figure 1 Effects of chronic exposure to rapamycin (Rp) on fuel secretagogue-induced insulin release from islets. (A) High (16·7 mM) glucose-induced and basal insulin release in control and Rp-treated islets. Islets were cultured with 10, 30, and 100 nM Rp or without Rp for 24 h. After cultured islets were preincubated with 2·8 mM glucose for 30 min, they were incubated with 2·8 and 16·7 mM glucose. Insulin secretions are presented as insulin secretion for 30 min/islet (right) and as the ratio of insulin secretion for 30 min to insulin content (left). Values represent mean±S.E.M. of 30 determinations. *$P<0·01$ versus corresponding control. (B) High KIC (16·7 mM)-induced and basal insulin release in control and Rp-treated islets. Islets were cultured with or without 30 nM Rp for 24 h. After cultured islets were preincubated with 2·8 mM glucose for 30 min, they were incubated with 2·8 and 16·7 mM KIC. Values represent mean±S.E.M. of 18 determinations. *$P<0·01$ versus corresponding control.

Table 1 Effect of chronic exposure to rapamycin on insulin content and DNA content. At the end of experiments indicated in Fig. 1A, insulin content and DNA content in islets were determined. Values represent mean±S.E.M. of 60 determinations

	Insulin content (ng/islet)	**DNA content** (ng/islet)
Experimental condition during culture		
Control	24·7±1·0	14·6±0·4
10 nM rapamycin	24·1±1·0	14·5±0·4
30 nM rapamycin	24·5±1·1	15·0±0·5
100 nM rapamycin	23·7±0·8	14·1±0·3

Effect of chronic exposure to rapamycin on KIC-induced insulin release

To characterize metabolic fuel-induced insulin release independent of glycolysis, KIC-induced insulin release from rapamycin-treated islets was examined. Chronic exposure to 30 nM rapamycin decreased high KIC-induced insulin release (1·93±0·10, rapamycin versus 3·09±0·18 ng/islet per 30 min, control, $n=18$, $P<0·01$; Fig. 1B).

Effect of rapamycin on ATP content

ATP content was greater in control islets incubated with 16·7 mM glucose than in control islets incubated with 2·8 mM glucose (11·97±0·35, 2·8 mM glucose versus 16·04±0·46 pmol/islet, 16·7 mM glucose, $n=30$, $P<0·01$; Fig. 2). ATP content in the presence of 16·7 mM glucose

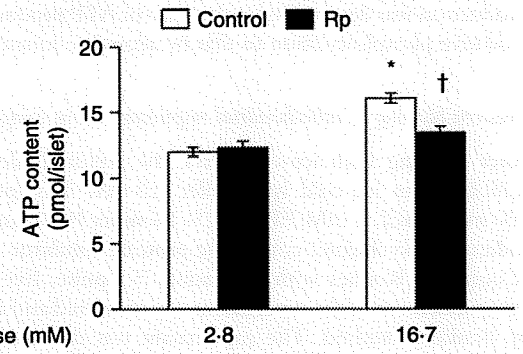

Figure 2 Effects of chronic exposure to rapamycin (Rp) on ATP contents in islets. Islets were cultured with or without 30 nM Rp for 24 h. After cultured islets were preincubated with 2·8 mM glucose for 30 min, and then incubated with 2·8 and 16·7 mM glucose for 30 min, ATP contents were determined. Values represent mean ±S.E.M. of 30 determinations. *$P<0·01$ versus control with 2·8 mM glucose. †$P<0·01$ versus control with 16·7 mM glucose.

was significantly reduced in rapamycin-treated islets (13·42 ±0·47 pmol/islet, 16·7 mM glucose, rapamycin versus 16·7 mM glucose, control, $n=30$, $P<0·01$), but that in the presence of 2·8 mM glucose was not affected by rapamycin (Fig. 2). ROS scavengers did not affect the suppressed ATP content in the presence of high glucose by rapamycin (13·27 ±0·92, 30 nM rapamycin versus 14·58±0·82 pmol/islet, 30 nM rapamycin with α-tocopherol plus ascorbate, $n=10$, not significant).

Effects of rapamycin on glucose utilization and glucose oxidation

Glucose utilization was greater in islets incubated with 16·7 mM glucose than that in islets incubated with 2·8 mM glucose in both control (33·0±1·8, 2·8 mM glucose versus 98·4±5·0 pmol/islet per 90 min, 16·7 mM glucose, $n=15$, $P<0·01$) and rapamycin-treated islets (28·1±1·7, 2·8 mM glucose versus 75·1±2·6 pmol/islet per 90 min, 16·7 mM glucose, $n=15$, $P<0·01$). Glucose utilization in the presence of 16·7 mM glucose was significantly reduced in rapamycin-treated islets ($P<0·01$), but that in the presence of 2·8 mM glucose was not affected by rapamycin (Fig. 3A).

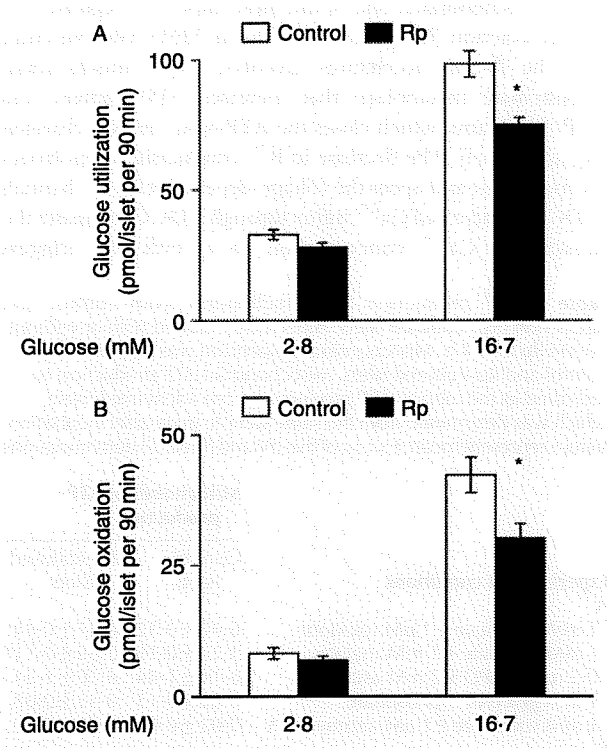

Figure 3 Effects of chronic exposure to rapamycin (Rp) on glucose utilization and oxidation in islets. Islets were cultured with or without 30 nM Rp for 24 h. After cultured islets were preincubated with 2·8 mM glucose for 30 min, they were incubated with 2·8 and 16·7 mM glucose for 90 min. (A) Glucose utilization. Values represent mean±S.E.M. of 15 determinations. *$P<0·01$ versus corresponding control. (B) Glucose oxidation. Values represent mean±S.E.M. of nine determinations. *$P<0·01$ versus corresponding control.

Glucose oxidation was greater in islets incubated with 16·7 mM glucose than that in islets incubated with 2·8 mM glucose in both control (8·1±1·1, 2·8 mM glucose versus 42·2±3·3 pmol/islet per 90 min, 16·7 mM glucose, $n=9$, $P<0·01$) and rapamycin-treated islets (6·8±0·7, 2·8 mM glucose versus 30·1±2·7 pmol/islet per 90 min, 16·7 mM glucose, $n=9$, $P<0·01$). Glucose oxidation in the presence of 16·7 mM glucose was significantly reduced in rapamycin-treated islets ($P<0·01$), but that in the presence of 2·8 mM glucose was not affected by rapamycin (Fig. 3B). Glucose oxidation in the presence of 16·7 mM glucose declined 77% by 100 nM antimycin A, which is comparable with the reduction by rapamycin treatment. In the same condition, glucose utilization with high glucose also declined 78% by antimycin A (Table 2).

Effect of rapamycin on glucokinase activity

Glucokinase activity was not affected by rapamycin treatment (87·4±10·4, rapamycin versus 75·4±14·8 pmol/islet per 60 min, control, $n=3$, not significant).

Effect of rapamycin on expression of mitochondrial respiratory chain complexes

Immunoblotting using lysates of whole islets revealed that rapamycin did not affect expression of complex I, III, IV, and V of the mitochondrial respiratory chain proteins (Fig. 4).

Effect of rapamycin on ATP production by mitochondria from islets

ATP production by mitochondria from control and rapamycin-cultured islets in the presence of various substrates and inhibitors is shown in Table 3. Antimycin A, a complex III inhibitor in the respiratory chain, inhibited ATP production dramatically in the presence of succinate in mitochondria from both control and rapamycin-cultured islets. Mitochondrial ATP production of rapamycin-cultured islets was similar to that of control islets in the presence of

Table 2 Effect of antimycin A on glucose oxidation and glucose utilization. Islets were cultured without rapamycin for 24 h. After cultured islets were preincubated with 2·8 mM glucose for 30 min, they were incubated with 2·8 and 16·7 mM glucose for 90 min with or without 100 nM antimycin A. Values represent mean±S.E.M. of nine (glucose oxidation) and five (glucose utilization) determinations

	Control	100 nM antimycin A
Glucose oxidation		
2·8 mM glucose	9·8±0·5	9·8±0·7
16·7 mM glucose	42·1±1·8	32·8±1·8*
Glucose utilization		
2·8 mM glucose	32·9±3·3	31·1±2·4
16·7 mM glucose	97·9±5·6	76·7±6·5†

*$P<0·01$ versus control without antimycin A. †$P<0·05$ versus control without antimycin A.

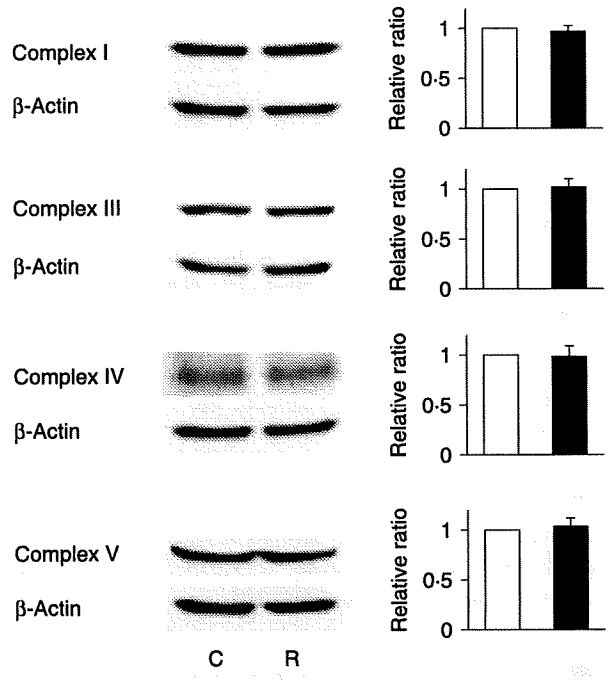

Figure 4 Immunoblots of complex I, III, VI, and V of mitochondrial respiratory chain proteins using lysates of whole-rat pancreatic islets. Islets were cultured with or without 30 nM rapamycin for 24 h. C, control; R, rapamycin. Quantification data from several independent experiments (I, $n=4$; III, $n=4$; VI, $n=3$; V, $n=4$) are also indicated. Open bar, control; closed bar, rapamycin. Data are expressed relative to control (without rapamycin) values corrected by β-actin level to eliminate influence of subtle difference in amount of loaded protein (means±S.E.M).

succinate plus rotenone, TMPD plus ascorbate, and glycerol-3-phosphate. ATP production by mitochondria from rapamycin-cultured islets in the presence of pyruvate plus malate was decreased compared with that from control islets.

α-Keto-β-methyl-*n*-valeric acid (KMV), a specific competitive inhibitor of KGDH, dose dependently suppressed mitochondrial ATP production in the presence of malate and pyruvate (Fig. 5).

Effect of rapamycin on activities of mitochondrial enzymes

Enzyme activities in the Krebs cycle including PDH, NAD-ICDH, aconitase, and MDH were not affected, but KGDH activity was reduced by rapamycin treatment (Table 4).

Discussion

In the present study, we show that rapamycin suppresses high glucose-induced insulin secretion from pancreatic islets by reducing mitochondrial ATP production through suppression of carbohydrate metabolism in the Krebs cycle, together with reduced KGDH activity. Thus, dysfunction in mitochondrial ATP production may be derived not from alteration in protein expression and dysfunction of the respiratory chain but from decreased KGDH activity that limits the velocity of carbohydrate metabolism in the Krebs cycle.

Rapamycin significantly decreased glucose-induced insulin release after 1 to several days exposure, as found in previous studies using rat islets (Bell *et al.* 2003) and mice islets (Zhang *et al.* 2006). In the present study, exposure to 30 nM rapamycin for 24 h reduced glucose-induced insulin release without affecting insulin and DNA content, which indicates that reduced insulin release by rapamycin is not necessarily derived from reduced β-cell mass, while rapamycin above 10 nM was found to increase apoptosis in MIN-6 cells in a previous study (Bell *et al.* 2003). To investigate the mechanism of reduced insulin release by rapamycin independent of reduced insulin and DNA content, we used 30 nM rapamycin-treated islets. The recommended trough concentrations of rapamycin in blood are 5–15 ng/ml (or 5·5–15·9 nM) in islet transplantation (Shapiro *et al.* 2000) and renal transplantation (Teutonico *et al.* 2005). Accordingly, the concentration used in our experiments was two to six times clinically used trough concentrations.

In pancreatic β-cells, intracellular ATP originated mainly from mitochondria is one of the most important regulators of insulin secretion (Maechler & Wollheim 2001). Glucose entry into the β-cells accelerates glycolysis and mitochondrial carbohydrate metabolism that increases ATP content and ATP/ADP ratio, which closes the ATP-sensitive K^+ channels (K_{ATP} channel). The decrease in K^+ conductance depolarizes the membrane and opens the voltage-dependent Ca^{2+} channels (VDCCs). Increased Ca^{2+} influx through VDCCs increases the intracellular Ca^{2+} concentration to a level that triggers

Table 3 ATP production by mitochondria from control and rapamycin (Rp)-cultured islets. Islets were cultured with or without 30 nM Rp for 24 h. Mitochondrial suspension was obtained from control and Rp-cultured islets. Mitochondrial ATP production is indicated as the ratio to ATP production from adenylate kinase, which was determined from the same sample in parallel incubation. Values represent mean±S.E.M. of five (A) and three (B) determinations

	Mitochondrial ATP production	
Experimental conditions	Control islets	Rp-cultured islets
A		
1 mM succinate+1 μM rotenone	6·40±0·32	6·47±0·44
1 mM pyruvate+1 mM malate	3·22±0·10	2·69±0·11*
0·5 mM TMPD+2 mM ascorbate	8·74±1·44	8·70±1·34
1 mM glycerol-3-phosphate	0·66±0·13	0·55±0·08
1 mM succinate+1 μM antimycin A	0·02±0·00	0·02±0·00
B		
1 mM succinate	7·13±0·12	ND
1 mM succinate+1 μM rotenone	6·39±0·06	ND
1 mM succinate+1 μM antimycin A	0·02±0·01	ND
1 mM succinate+1 μM rotenone+1 μM antimycin A	0·03±0·00	ND

*$P<0·05$ versus corresponding control cultured without Rp. TMPD, tetramethyl-*p*-phenyldiamine. ND, not determined.

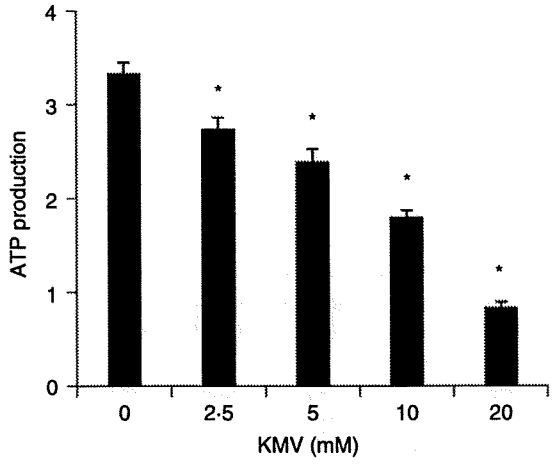

Figure 5 Effect of α-keto-β-methyl-*n*-valeric acid (KMV) on mitochondrial ATP production. Islets were cultured for 24 h. Mitochondrial suspension was obtained from cultured islets. Mitochondrial ATP production in the presence of 1 mM pyruvate and 1 mM malate with various concentrations of KMV is indicated as the ratio to ATP production from adenylate kinase, which was determined from the same sample in parallel incubation. Values represent mean±S.E.M. of six determinations. *$P<0·01$ versus control without KMV.

exocytosis of the insulin granules. Moreover, ATP directly affects the exocytotic system and enhances insulin release in experiments using single β-cells (Rorsman 1997, Takahashi *et al.* 1999) and permeabilized islets (Fujimoto *et al.* 2002). Thus, a lower ATP level in the presence of high glucose plays a major role in the attenuation of insulin secretion from rapamycin-treated islets in response to high glucose.

In pancreatic islets, KIC is oxidized, enhancing ATP production and triggering insulin release (Malaisse *et al.* 1981), and two distinct mechanisms of KIC-induced insulin release are proposed. In one, KIC, which is converted to acetyl CoA via a branched chain α-keto acid dehydrogenase (BCKDH) -dependent pathway, enters into the Krebs cycle and is oxidized (Lenzen *et al.* 1982, 1985). In the other, KIC together with endogenous glutamate is converted to α-ketoglutarate via glutamate-keto acid transaminase (GKAT), which enters into the Krebs cycle and is oxidized (Gao *et al.* 2003). Because both BCKDH and GKAT are mitochondrial enzymes, KIC might well be metabolized within mitochondria without affecting cytosolic glycolysis, which is compatible with the results showing that inhibition of glycolysis by glucokinase inhibitor and glyceraldehyde-3-phosphate dehydrogenase inhibitor decreased glucose-induced insulin release, but did not affect KIC-induced insulin release (Radu *et al.* 2005). Reduced KIC-induced insulin release by rapamycin suggests that the decreased glucose metabolism may be derived from reduced mitochondrial carbohydrate metabolism.

Table 4 Effect of rapamycin (Rp) on enzyme activities in the Krebs cycle. Islets were cultured with or without 30 nM Rp for 24 h. Enzyme activities were measured using homogenates of mitochondrial fraction obtained from control and Rp-cultured islets. Values represent mean±S.E.M. of five determinations

	Enzyme activities (nmol/mg mitochondrial protein per min)	
	Control islets	Rp-cultured islets
PDH	10·64±0·38	10·98±0·38
Aconitase	10·83±0·78	9·77±0·78
NAD-ICDH	11·50±0·28	10·99±0·30
KGDH	13·82±0·84	10·08±0·82*
MDH	1116±37	1127±37

*$P<0·05$ versus corresponding control cultured without Rp. PDH, pyruvate dehydrogenase; NAD-ICDH, NAD^+ linked-isocitrate dehydrogenase; KGDH, α-ketoglutarate dehydrogenase; MDH, malate dehydrogenase.

Because rapamycin reduced glucose utilization in the presence of high glucose, which reflects the velocity of glycolysis (Meglasson & Matschinsky 1986), the activity of glucokinase, a rate-limiting enzyme in glycolysis (Matschinsky 1996), was examined. Since rapamycin treatment did not affect glucokinase activity in islets, the primary cause of reduced glucose oxidation by the treatment is not likely to be reduced the velocity of glycolysis. Indeed, in islets, glucose utilization is also reduced when glucose oxidation is decreased by respiratory chain inhibitors including site III inhibitor in our results and site VI inhibitor (Sener *et al.* 2007), suggesting that reduced glucose oxidation may decrease glucose utilization. Since glucokinase is a unique hexokinase, which lacks product inhibition (Matschinsky 2002), accumulation of glucose-6-phosphate by mitochondrial metabolic inhibition may not participate in glycolysis inhibition. Moreover, since K_m of glucokinase for ATP is about 0·5 mM, which is less than the estimated cytosolic ATP concentration with a basal level of glucose in β-cells (about 3 mM; Meglasson & Matschinsky 1984), a decrease in the cytosolic ATP concentration by mitochondrial metabolic inhibition may have little effect on velocity of glycolysis.

Mitochondrial ATP production is driven by the H^+ gradient across the mitochondrial membrane generated by transport of high-energy electrons in the respiratory chain. These electrons are derived from NADH and $FADH_2$ derived from the Krebs cycle in the matrix and/or transferred from the cytosol by the shuttle system. To find the defective site in mitochondrial carbohydrate metabolism in rapamycin-cultured islets, mitochondrial ATP production was examined in the presence of various substrates and inhibitors. As ATP production in the presence of glycerol phosphate was not affected, reduced function of the glycerol phosphate shuttle, which is observed in diabetic islets (Östenson *et al.* 1993), may not participate in the reduction of ATP production by rapamycin treatment. In the presence of rotenone, a complex I inhibitor, and succinate, which renders electrons indirectly to complex I via the Krebs cycle and directly to complex II, electrons are rendered to the respiratory chain via $FADH_2$ at complex II and not at complex I via NADH, which is derived from metabolism in the Krebs cycle. TMPD is an artificial

electron donor that can transfer electrons to cytochrome *c*. TMPD reduced by ascorbate renders electrons to cytochrome *c*, which transfers electrons to complex IV. The fact that ATP production in the presence of succinate plus rotenone and in the presence of TMPD plus ascorbate is similar in the two groups of mitochondria indicates that the respiratory chain downstream of complex II is not affected by chronic exposure to rapamycin. Moreover, immunoblotting revealed that expressions of respiratory chain proteins including complex I, III, IV, and V were not affected by rapamycin treatment. Antibodies used in the present study were raised against 39 kDa subunit in complex I, core II in complex III, subunit I in complex IV, and subunit α in complex V. In these subunits, subunit I in complex IV is derived from an mtDNA-encoded gene; the others are from nuclear genes (Hunte 2001, Richter & Ludwig 2003, Scheffler 2008, Zickermann *et al.* 2009), indicating that rapamycin does not affect the expression of respiratory proteins derived from mtDNA or nuclear genes in islets. Considered together, these results do not support the notion that rapamycin reduces ATP production by reducing activity of the respiratory chain. Because the decrease in ATP production was found in the presence of substrates that are metabolizable in the Krebs cycle by rapamycin treatment, the reduction in ATP production may be attributable to reduced carbohydrate metabolism in the Krebs cycle.

Glucose oxidation reflects the velocity of carbohydrate metabolism in the Krebs cycle in which CO_2 is released in the reaction mediated by dehydrogenases. To clarify the link between reduced mitochondrial ATP production in the presence of substrates metabolizable in the Krebs cycle and reduced glucose oxidation by rapamycin, recovery of insulin release and ATP content in the presence of high glucose by ROS scavengers and activity of enzymes in the Krebs cycle were examined. Ouabain-induced endogenous ROS suppresses mitochondrial metabolism in the Krebs cycle, subsequently reducing ATP production, and reduces glucose-induced insulin release and ATP levels in the presence of high glucose, which is recovered by the suppression of endogenous ROS production and by ROS scavenge (Kajikawa *et al.* 2002, Kominato *et al.* 2008). High glucose raises ROS level in β-cells (Bindokas *et al.* 2003, Sakai *et al.* 2003), which is also found in our previous study (Kominato *et al.* 2008). However, our previous study shows that ROS scavenging does not affect glucose-induced insulin secretion from control islets, but increases that from GK-diabetic islets. A more profound increase in high glucose-induced ROS was observed in diabetic islets compared with control islets. These results suggest that a physiological level of ROS increase by glucose does not impair stimulus-secretion coupling, while a pathophysiological increase in ROS impairs stimulus-secretion coupling. Administration of H_2O_2, the most abundant ROS, to mitochondria reduced the activity of Krebs cycle enzymes including aconitase, KGDH, and succinate dehydrogenase (Tretter & Adam-Vizi 2000, Nulton-Persson & Szweda 2001). Because α-tocopherol is a lipid-soluble antioxidant, it is often used as membrane-permeable ROS scavenger. α-tocopherol reduces ROS production in various kinds of cells (Saito *et al.* 2003, Brookheart *et al.* 2009, Yang *et al.* 2009) including β-cells (Kajikawa *et al.* 2002). As ascorbate is water soluble, it is not necessarily membrane permeable. However, it is useful to prevent oxidization of α-tocopherol in the medium and to maintain the ROS-scavenging effect of α-tocopherol. Because insulin release and ATP content in the presence of high glucose in rapamycin-treated islets were not increased by the addition of α-tocopherol plus ascorbate, overproduction of endogenous ROS seems not to participate in reduced mitochondrial carbohydrate metabolism due to rapamycin treatment.

Impaired metabolism-secretion coupling in β-cells due to reduced activity of enzymes in the Krebs cycle has been reported. Exposure to fatty acids for 48 h inhibits glucose-induced insulin secretion from islets with decreased activity in PDH (Zhou & Grill 1995). Interleukin-1β-induced nitric oxide production leads to inhibition of glucose-induced insulin secretion together with reduced aconitase activity (Welsh *et al.* 1991). In the present study, activity of KGDH was decreased by rapamycin treatment. The reaction catalyzed by KGDH is one of the slowest steps in the Krebs cycle, and thus can be the rate-limiting step in islets (Ashcroft 1981) and in other tissues (Tretter & Adam-Vizi 2000, Nulton-Persson & Szweda 2001). Inhibition of KGDH alters mitochondrial function in N2a neuroblastoma cells (Huang *et al.* 2003). These findings suggest that decreased activity of KGDH might reduce mitochondrial ATP production and result in decreased glucose-induced insulin secretion from rapamycin-treated islets. To investigate this, suppression of mitochondrial ATP production by inhibition of KGDH was examined using KMV, a specific competitive inhibitor of KGDH (Huang *et al.* 2003). KMV dose dependently suppressed mitochondrial ATP production in the presence of malate and pyruvate. This dose dependency of KMV on mitochondrial ATP production is consistent with the dose-dependent effect of KMV on KGDH activities previously described (Huang *et al.* 2003). These results indicate that reaction at KGDH may limit the velocity of carbohydrate metabolism in the Krebs cycle and thus mitochondrial ATP production, which is consistent with the result that KGDH limits the amount of NADH available for the respiratory chain (Tretter & Adam-Vizi 2000). These results support the notion that a slight alteration in KGDH activity may affect mitochondrial ATP production.

While rapamycin shares with tacrolimus a similar molecular structure and binding ability to FK-binding protein 12 (FKBP12), the FKBP12–rapamycin complex has no effect on calcineurin, a phosphatase that is known to be inhibited by the FKBP12–tacrolimus complex (Saunders *et al.* 2001). This is consistent with our finding in the present study that rapamycin had no effect on glucokinase activity, but tacrolimus suppresses glucokinase activity in islets (Radu *et al.* 2005). MTOR has an FKBP12–rapamycin binding domain to which phosphatidic acid (PA) can also bind.

MTOR expresses biological effects by forming two types of complexes, MTORC1 and MTORC2, which includes MTOR and PA commonly and Raptor and Rictor respectively. FKBP12–rapamycin is believed to inhibit MTOR signaling by preventing the interaction between MTOR and PA and thus forming MTOR complexes (Foster & Toschi 2009). Since low concentrations of rapamycin (0·5–100 nM) target MTORC1 and higher concentrations of rapamycin (0·2–20 μM) target MTORC2 (Foster & Toschi 2009), our result may be derived from inhibition of signaling mediated by MTORC1.

Recently, it has been revealed that MTOR is a nutrient sensor that balances energy metabolism by transcriptional control of mitochondrial oxidative function using peroxisome proliferator-activated receptor γ coactivator-1α in skeletal muscle cells (Cunningham *et al.* 2007). Further investigation of suppression of KGDH activity by rapamycin is required to clarify adaptation of mitochondrial oxidative function and insulin secretion according to nutrient supply.

Declaration of interest

The authors declare that there is no conflict of interest that would prejudice the impartiality of this scientific work.

Funding

This study was supported by Scientific Research Grants, a Grant for Leading Project for Biosimulation from the Ministry of Education, Culture, Sports, Science, and Technology of Japan, and a grant from CREST of Japan Science and Technology Cooperation.

Acknowledgements

The authors thank Mr T Yamaguchi and Ms C Kotake for their technical assistance.

References

Ashcroft SJH 1981 Metabolic control of insulin secretion. In *The Islets of Langerhans: Biochemistry, Physiology, and Pathology*, pp 117–148. Eds SJ Cooperstein & D Watkins. New York: Academic Press.

Bell E, Cao X, Moibi JA, Greene SR, Young R, Trucco M, Gao Z, Matschinsky FM, Deng S, Markman JF *et al.* 2003 Rapamycin has a deleterious effect on MIN-6 cells and rat and human islets. *Diabetes* **52** 2731–2739.

Bindokas VP, Kuznetsov A, Sreenan S, Polonsky KS, Roe MW & Philipson LH 2003 Visualizing superoxide production in normal and diabetic rat islets of Langerhans. *Journal of Biological Chemistry* **278** 9796–9801.

Brookheart RT, Michel CI, Listenberger LL, Ory DS & Schaffer JE 2009 The non-coding RNA gadd7 is a regulator of lipid-induced oxidative and endoplasmic reticulum stress. *Journal of Biological Chemistry* **284** 7446–7454.

Cho HJ, Park J, Lee HW, Lee YS & Kim JB 2004 Regulation of adipocyte differentiation and insulin action with rapamycin. *Biochemical and Biophysical Research Communications* **321** 942–948.

Cunningham JT, Rodgers JT, Arlow DH, Vazquez F, Mootha VK & Puigserver P 2007 mTOR controls mitochondrial oxidative function through a YY1-PGC-1α transcriptional complex. *Nature* **450** 736–740.

Foster DA & Toschi A 2009 Targeting mTOR with rapamycin: one dose does not fit all. *Cell Cycle* **8** 1026–1029.

Fraenkel M, Ketzinel-Gilad M, Ariav Y, Pappo O, Karaca M, Castel J, Berthault MF, Magnan C, Cerasi E, Kaiser N *et al.* 2008 mTOR inhibition by rapamycin prevents β-cell adaptation to hyperglycemia and exacerbates the metabolic state in type 2 diabetes. *Diabetes* **57** 945–957.

Fujimoto S, Ishida H, Kato S, Okamoto Y, Tsuji K, Mizuno N, Ueda S, Mukai E & Seino Y 1998 The novel insulinotropic mechanism of pimobendan: direct enhancement of the exocytotic process of insulin secretory granules by increased Ca^{2+} sensitivity in β-cells. *Endocrinology* **139** 1133–1140.

Fujimoto S, Tsuura Y, Ishida H, Tsuji K, Mukai E, Kajikawa M, Hamamoto Y, Takeda T, Yamada Y & Seino Y 2000 Augmentation of basal insulin release from rat islets by preexposure to a high concentration of glucose. *American Journal of Physiology* **279** E927–E940.

Fujimoto S, Mukai E, Hamamoto Y, Takeda T, Takehiro M, Yamada Y & Seino Y 2002 Prior exposure to high glucose augments depolarization-induced insulin release by mitigating the decline of ATP level in rat islets. *Endocrinology* **143** 213–221.

Fujimoto S, Nabe K, Takehiro M, Shimodahira M, Kajikawa M, Takeda T, Mukai E, Inagaki N & Seino Y 2007 Impaired metabolism-secretion coupling in pancreatic β-cells: role of determinants of mitochondrial ATP production. *Diabetes Research and Clinical Practice* **77** S2–S10.

Gao Z, Young RA, Li G, Najafi H, Buettger C, Sukumvanich SS, Wong RK, Wolf BA & Matschinsky FM 2003 Distinguishing features of leucine and α-ketoisocaproate sensing in pancreatic β-cells. *Endocrinology* **144** 1949–1957.

Huang HM, Zhang H, Xu H & Gibson GE 2003 Inhibition of the α-ketoglutarate dehydrogenase complex alters mitochondrial function and cellular calcium regulation. *Biochimica et Biophysica Acta* **1637** 119–126.

Hunte C 2001 Insights from the structure of the yeast cytochrome bc1 complex: crystallization of membrane proteins with antibody fragments. *FEBS Letters* **504** 126–132.

Kajikawa M, Fujimoto S, Tsuura Y, Mukai E, Takeda T, Hamamoto Y, Takehiro M, Fujita J, Yamada Y & Seino Y 2002 Ouabain suppresses glucose-induced mitochondrial ATP production and insulin release by generating reactive oxygen species in pancreatic islets. *Diabetes* **51** 2522–2529.

Kennedy ED, Maechler P & Wollheim CB 1998 Effects of depletion of mitochondrial DNA in metabolism secretion coupling in INS-1 cells. *Diabetes* **47** 374–380.

Kominato R, Fujimoto S, Mukai E, Nakamura Y, Nabe K, Shimodahira M, Nishi Y, Funakoshi S, Seino Y & Inagaki N 2008 Src activation generates reactive oxygen species and impairs metabolism-secretion coupling in diabetic Goto-Kakizaki and ouabain-treated rat pancreatic islets. *Diabetologia* **51** 1226–1235.

Lenzen S, Formanek H & Panten U 1982 Signal function of metabolism of neutral amino acids and 2-keto acids for initiation of insulin secretion. *Journal of Biological Chemistry* **257** 6631–6633.

Lenzen S, Schmidt W & Panten U 1985 Transamination of neutral amino acids and 2-keto acids in pancreatic B-cell mitochondria. *Journal of Biological Chemistry* **260** 12629–12634.

Lu X, Schuurman HJ & Borel JF 1994 Effect of rapamycin on islet xenograft survival. *Transplantation Proceedings* **26** 1128–1129.

Maechler P & Wollheim CB 2001 Mitochondrial function in normal and diabetic β-cells. *Nature* **414** 807–812.

Malaisse WJ, Sener A, Malaisse-Legae F, Hutton JC & Christophe J 1981 The stimulus-secretion coupling of amino acid-induced insulin release. Metabolic interaction of L-glutamine and 2-ketoisocaproate in pancreatic islets. *Biochimica et Biophysica Acta* **677** 39–49.

Matschinsky FM 1996 Banting Lecture 1995. A lesson in metabolic regulation inspired by the glucokinase glucose sensor paradigm. *Diabetes* **45** 223–241.

Matschinsky FM 2002 Regulation of pancreatic β-cell glucokinase. *Diabetes* **51** S394–S404.

McDaniel ML, Marshall CA, Pappan KL & Kwon G 2002 Metabolic and autocrine regulation of the mammalian target of rapamycin by pancreatic β-cells. *Diabetes* **51** 2877–2885.

Meglasson MD & Matschinsky FM 1984 New perspectives on pancreatic islet glucokinase. *American Journal of Physiology* **246** E1–E13.

Meglasson MD & Matschinsky FM 1986 Pancreatic islet glucose metabolism and regulation of insulin secretion. *Diabetes/Metabolism Reviews* **2** 163–214.

Nabe K, Fujimoto S, Shimodahira M, Kominato R, Nishi Y, Funakoshi S, Mukai E, Yamada Y, Seino Y & Inagaki N 2006 Diphenylhydantoin suppresses glucose-induced insulin release by decreasing cytoplasmic H^+ concentration in pancreatic islets. *Endocrinology* **147** 2717–2727.

Nulton-Persson AC & Szweda LI 2001 Modulation of mitochondrial function by hydrogen peroxide. *Journal of Biological Chemistry* **276** 23357–23361.

Östenson CG, Abdel-Halim SM, Rasschaert J, Malaisse-Lagae F, Meuris S, Sener A, Efendic S & Malaisse WJ 1993 Deficient activity of FAD-linked glycerophosphate dehydrogenase in islets of GK rats. *Diabetologia* **36** 722–726.

Radu RG, Fujimoto S, Mukai E, Takehiro M, Shimono D, Nabe K, Shimodahira M, Kominato R, Aramaki Y, Nishi Y *et al.* 2005 Tacrolimus suppresses glucose-induced insulin release from pancreatic islets by reducing glucokinase activity. *American Journal of Physiology* **288** E372–E380.

Richter OM & Ludwig B 2003 Cytochrome *c* oxidase – structure, function, and physiology of a redox-driven molecular machine. *Reviews of Physiology, Biochemistry and Pharmacology* **147** 47–74.

Rorsman P 1997 The pancreatic β-cell as a fuel sensor: an electrophysiologist's viewpoint. *Diabetologia* **40** 487–495.

Saito Y, Yoshida Y, Akazawa T, Takahashi K & Niki E 2003 Cell death caused by selenium deficiency and protective effect of antioxidants. *Journal of Biological Chemistry* **278** 39428–39434.

Sakai K, Matsumoto K, Nishikawa T, Suefuji M, Nakamaru K, Hirashima Y, Kawashima J, Shirotani T, Ichinose K, Brownlee M *et al.* 2003 Mitochondrial reactive oxygen species reduce insulin secretion by pancreatic β-cells. *Biochemical and Biophysical Research Communications* **300** 216–222.

Saunders RN, Metcalfe MS & Nicholson ML 2001 Rapamycin in transplantation: a review of the evidence. *Kidney International* **59** 3–16.

Scheffler IE 2008 Biogenesis of mitochondria and mitochondrial electron transfer and oxidative phosphorylation. In *Mitochondria*, edn 2, pp 60–297. Ed. IE Scheffler. Hoboken: John Wiley & Sons, Inc.

Schieke SM, Phillips D, McCoy JP Jr, Aponte AM, Shen RF, Balaban RS & Finkel T 2006 The mammalian target of rapamycin (mTOR) pathway regulates mitochondrial oxygen consumption and oxidative capacity. *Journal of Biological Chemistry* **281** 27643–27652.

Schwab MA, Kölker S, van den Heuvel LP, Sauer S, Wolf NI, Rating D, Hoffmann GF, Smeitink JA & Okun JG 2005 Optimized spectrophotometric assay for the completely activated pyruvate dehydrogenase complex in fibroblasts. *Clinical Chemistry* **51** 151–160.

Sener A, Jijakli H, Zahedi Asl S, Courtois P, Yates AP, Meuris S, Best LC & Malaisse WJ 2007 Possible role of carbonic anhydrase in rat pancreatic islets: enzymatic, secretory, metabolic, ionic, and electrical aspects. *American Journal of Physiology* **292** E1624–E1630.

Shapiro AM, Lakey JR, Ryan EA, Korbutt GS, Toth E, Warnock GL, Kneteman NM & Rajotte RV 2000 Islet transplantation in seven patients with type 1 diabetes mellitus using a glucocorticoid-free immunosuppressive regimen. *New England Journal of Medicine* **343** 230–238.

Simon N, Morin C, Urien S, Tillement JP & Bruguerolle B 2003 Tacrolimus and sirolimus decrease oxidative phosphorylation of isolated rat kidney mitochondria. *British Journal of Pharmacology* **138** 369–376.

Sipula IJ, Brown NF & Perdomo G 2006 Rapamycin-mediated inhibition of mammalian target of rapamycin in skeletal muscle cells reduces glucose utilization and increases fatty acid oxidation. *Metabolism* **55** 1637–1644.

Taha C, Liu Z, Jin J, Al-Hasani H, Sonenberg N & Klip A 1999 Opposite translational control of GLUT1 and GLUT4 glucose transporter mRNAs in response to insulin. Role of mammalian target of rapamycin, protein kinase B, and phosphatidylinositol 3-kinase in GLUT1 mRNA translation. *Journal of Biological Chemistry* **274** 33085–33091.

Takahashi N, Kadowaki T, Yazaki Y, Ellis-Davies GC, Miyashita Y & Kasai H 1999 Post-priming actions of ATP on Ca^{2+}-dependent exocytosis in pancreatic β cells. *PNAS* **96** 760–765.

Takehiro M, Fujimoto S, Shimodahira M, Shimono D, Mukai E, Nabe K, Radu RG, Kominato R, Aramaki Y, Seino Y *et al.* 2005 Chronic exposure to β-hydroxybutyrate inhibits glucose-induced insulin release from pancreatic islets by decreasing NADH contents. *American Journal of Physiology* **288** E365–E371.

Teutonico A, Schena PF & Di Paolo S 2005 Glucose metabolism in renal transplant recipients: effect of calcineurin inhibitor withdrawal and conversion to sirolimus. *Journal of the American Society of Nephrology* **16** 3128–3135.

Tretter L & Adam-Vizi V 2000 Inhibition of Krebs cycle enzymes by hydrogen peroxide: a key role of α-ketoglutarate dehydrogenase in limiting NADH production under oxidative stress. *Journal of Neuroscience* **20** 8972–8979.

Tsuruzoe K, Araki E, Furukawa N, Shirotani T, Matsumoto K, Kaneko K, Motoshima H, Yoshizato K, Shirakami A, Kishikawa H *et al.* 1998 Creation and characterization of a mitochondrial DNA-depleted pancreatic β-cell line: impaired insulin secretion induced by glucose, leucine, and sulfonylureas. *Diabetes* **47** 621–631.

Welsh N, Eizirik DL, Bendtzen K & Sandler S 1991 Interleukin-1 β-induced nitric oxide production in isolated rat pancreatic islets requires gene transcription and may lead to inhibition of the Krebs cycle enzyme aconitase. *Endocrinology* **129** 3167–3173.

Yang ZC, Wang KS, Wu Y, Zou XQ, Xiang YY, Chen XP & Li YJ 2009 Asymmetric dimethylarginine impairs glucose utilization via ROS/TLR4 pathway in adipocytes: an effect prevented by vitamin E. *Cellular Physiology and Biochemistry* **24** 115–124.

Zhang N, Su D, Qu S, Tse T, Bottino R, Balamurugan AN, Xu J, Bromberg JS & Dong HH 2006 Sirolimus is associated with reduced islet engraftment and impaired β-cell function. *Diabetes* **55** 2429–2436.

Zhou YP & Grill V 1995 Long term exposure to fatty acids and ketones inhibits B-cell functions in human pancreatic islets of Langerhans. *Journal of Clinical Endocrinology and Metabolism* **80** 1584–1590.

Zickermann V, Kerscher S, Zwicker K, Tocilescu MA, Radermacher M & Brandt U 2009 Architecture of complex I and its implications for electron transfer and proton pumping. *Biochimica et Biophysica Acta* **1787** 574–583.

Received in final form 16 September 2009
Accepted 7 October 2009
Made available online as an Accepted Preprint
7 October 2009

Biochemical and Biophysical Research Communications 389 (2009) 523–526

Contents lists available at ScienceDirect

Biochemical and Biophysical Research Communications

journal homepage: www.elsevier.com/locate/ybbrc

GLP-1 receptor antagonist as a potential probe for pancreatic β-cell imaging

Eri Mukai [a,b], Kentaro Toyoda [a], Hiroyuki Kimura [c], Hidekazu Kawashima [d], Hiroyuki Fujimoto [a,b], Masashi Ueda [e], Takashi Temma [c], Konomu Hirao [f], Kenji Nagakawa [f], Hideo Saji [c], Nobuya Inagaki [a,g,*]

[a] Department of Diabetes and Clinical Nutrition, Graduate School of Medicine, Kyoto University, Kyoto, Japan
[b] Japan Association for the Advancement of Medical Equipment, Tokyo, Japan
[c] Department of Patho-Functional Bioanalysis, Graduate School of Pharmaceutical Sciences, Kyoto University, Kyoto, Japan
[d] Department of Diagnostic Imaging and Nuclear Medicine, Graduate School of Medicine, Kyoto University, Kyoto, Japan
[e] Radioisotopes Research Laboratory, Kyoto University Hospital, Faculty of Medicine, Kyoto University, Kyoto, Japan
[f] Research & Development Division, Arkray, Inc., Kyoto, Japan
[g] CREST of Japan Science and Technology Cooperation (JST), Kyoto, Japan

ARTICLE INFO

Article history:
Received 2 September 2009
Available online 6 September 2009

Keywords:
Glucagon-like peptide-1
Glucagon-like peptide-1 receptor
Exendin-4
Exendin(9-39)
β-Cell imaging
Islet imaging
Molecular imaging
β-Cell mass
Diabetes

ABSTRACT

We examined exendin(9-39), an antagonist of glucagon-like peptide-1 (GLP-1) receptor (GLP-1R), as a potential probe for imaging of pancreatic β-cells. To evaluate *in vitro* receptor specificity, binding assay was performed using dispersed mouse islet cells. Binding assay showed competitive inhibition of [^{125}I]BH-exendin(9-39) binding by non-radioactive exendin(9-39). To assess *in vivo* selectivity, the biodistribution was evaluated by intravenous administration of [^{125}I]BH-exendin(9-39) to mice. Radioactivity of harvested pancreas reached highest levels at 60 and 120 min among organs examined except lung. Pre-administration of excess non-radioactive exendin(9-39) remarkably and specifically blocked the radioactivity of pancreas. After [^{125}I]BH-exendin(9-39) injection into transgenic mice with pancreatic β-cells expressing GFP, fluorescent and radioactive signals of sections of pancreas were evaluated with an image analyzer. Imaging analysis showed that the fluorescent GFP signals and the radioactive signals were correspondingly located. Thus, the GLP-1R antagonist exendin(9-39) may serve as a useful probe for pancreatic β-cell imaging.

Introduction

Type 1 diabetes is an autoimmune disease in which the pancreatic β-cells are almost destroyed, which leads to loss of endogenous insulin secretion. Insulin therapy is therefore required for survival in subjects with type 1 diabetes [1]. Type 2 diabetes is characterized by impaired insulin secretion and insulin resistance, and the pathogenesis is well known to be dependent on a reduction in β-cell function [2]. While a decrease in β-cell mass has been reported in American and Asian type 2 diabetic subjects compared with non-diabetic subjects [3–5], the decrease is small at onset in European subjects, suggesting that the decrease might occur only after onset of the disease [6]. It is therefore unknown whether a decrease in β-cell mass contributes to the development of hyperglycemia that leads to type 2 diabetes. Thus, accurately measuring changes in β-cell mass *in vivo* during diabetes progression is important not only for understanding the pathogenesis but also for facilitating early diagnosis and developing improved treatments for both type 1 and type 2 diabetes.

* Corresponding author. Address: Department of Diabetes and Clinical Nutrition, Graduate School of Medicine, Kyoto University, 54 Shogoin Kawahara-cho, Sakyo-ku, Kyoto 606-8507, Japan. Fax: +81 75 771 6601.
E-mail address: inagaki@metab.kuhp.kyoto-u.ac.jp (N. Inagaki).

0006-291X/$ - see front matter © 2009 Elsevier Inc. All rights reserved.
doi:10.1016/j.bbrc.2009.09.014

However, it is difficult to identify islets ranging in size from 50–500 μm in diameter and scattered throughout the pancreas, which is surrounded by abdominal organs. To quantify β-cell mass non-invasively, appropriate probes that can specifically bind to pancreatic β-cells are required. There are previous reports using probes targeting the proteins in β-cells, including sulfonylurea receptor 1 (SUR1) and monoamine transporter 2 (VMAT2) for positron emission tomography (PET) imaging [7]. However, ideal probes for accurate and non-invasive imaging for pancreatic β-cells have not yet been developed.

Glucagon-like peptide 1 (GLP-1) is the incretin peptide released from the intestine in response to nutrient ingestion to augment glucose-induced insulin secretion from pancreatic β-cells through binding to the GLP-1 receptor (GLP-1R) [8,9]. Since GLP-1R is expressed highly in islets, especially on β-cells in pancreas, the ligands of GLP-1R might well be ideal probes for pancreatic β-cell imaging. Because native GLP-1 is degraded rapidly by dipeptidyl peptidase-IV (DPP-IV) distributed throughout the body, DPP-IV-resistant agonistic or antagonistic ligands of GLP-1R [10,11] are preferable to GLP-1 for use as an imaging probe.

In the present study, specific imaging of pancreatic β-cells targeting GLP-1R was evaluated using its antagonist, exendin(9-39), radiolabeled with [^{125}I]-Bolton-Hunter reagent at lysine residues.

Materials and methods

Radiolabeling of exendin(9-39). [^{125}I]-Bolton-Hunter-labeled exendin(9-39) ([^{125}I]-BH exendin(9-39)) was purchased from Perkin-Elmer (Waltham, MA).

Animals. Six-week-old male ddY mice were obtained from Shimizu Co. (Kyoto, Japan). Transgenic mice expressing green fluorescent protein (GFP) under control of the mouse insulin I gene promoter (MIP) (MIP-GFP mice) were maintained on a C57BL/6 background [12]. Animal care and procedures were approved by the Animal Care Committee of Kyoto University.

Binding assay. The displacing effect of exendin(9-39) on GLP-1R binding was assessed using dispersed islet cells as described previously [13]. Pancreatic islets were isolated from male ddY mice by a collagenase digestion technique [14]. Isolated islets were dispersed using 0.05% trypsin/0.53 mM EDTA (Invitrogen, Carlsbad, CA) and PBS. Islet cells were incubated with [^{125}I]BH-exendin(9-39) (0.1 μCi) in 1 ml of buffer containing 20 mM Hepes (pH 7.4), 1 mM $MgCl_2$, 1 mg/ml bacitracin, and 1 mg/ml BSA for 1 h at room temperature in the presence of varying concentrations of non-radioactive exendin(9-39). Binding was terminated by rapid filtration through Whatman GF/C filters (24 mm) followed by washing three times with 5 ml of ice-cold PBS. The radioactivity of filters was measured in a γ-counter. Results were expressed as the percent radioactivity of bound [^{125}I]BH-exendin(9-39) that remained after addition of non-radioactive compound.

Biodistribution experiments. Biodistribution studies of [^{125}I]BH-exendin(9-39) were performed in male ddY mice. [^{125}I]BH-exendin(9-39) (1 μCi) was administered by tail vein injection. At 15, 30, 60, and 120 min after administration, the mice were sacrificed by exsanguination under anesthesia. Selected organs and blood

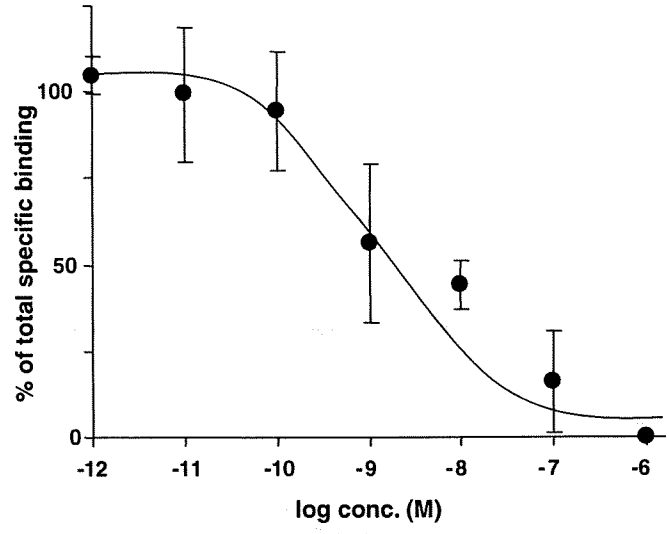

Fig. 1. Binding assay analysis of [^{125}I]BH-exendin(9-39) using mouse pancreatic islet cells. Competitive inhibition of [^{125}I]BH-exendin(9-39) binding by non-radioactive exendin(9-39) is shown. Values are expressed as means ± SD of the percent radioactivity of bound [^{125}I]BH-exendin(9-39) that remained after addition of indicated concentrations of non-radioactive exendin(9-39) (n = 4).

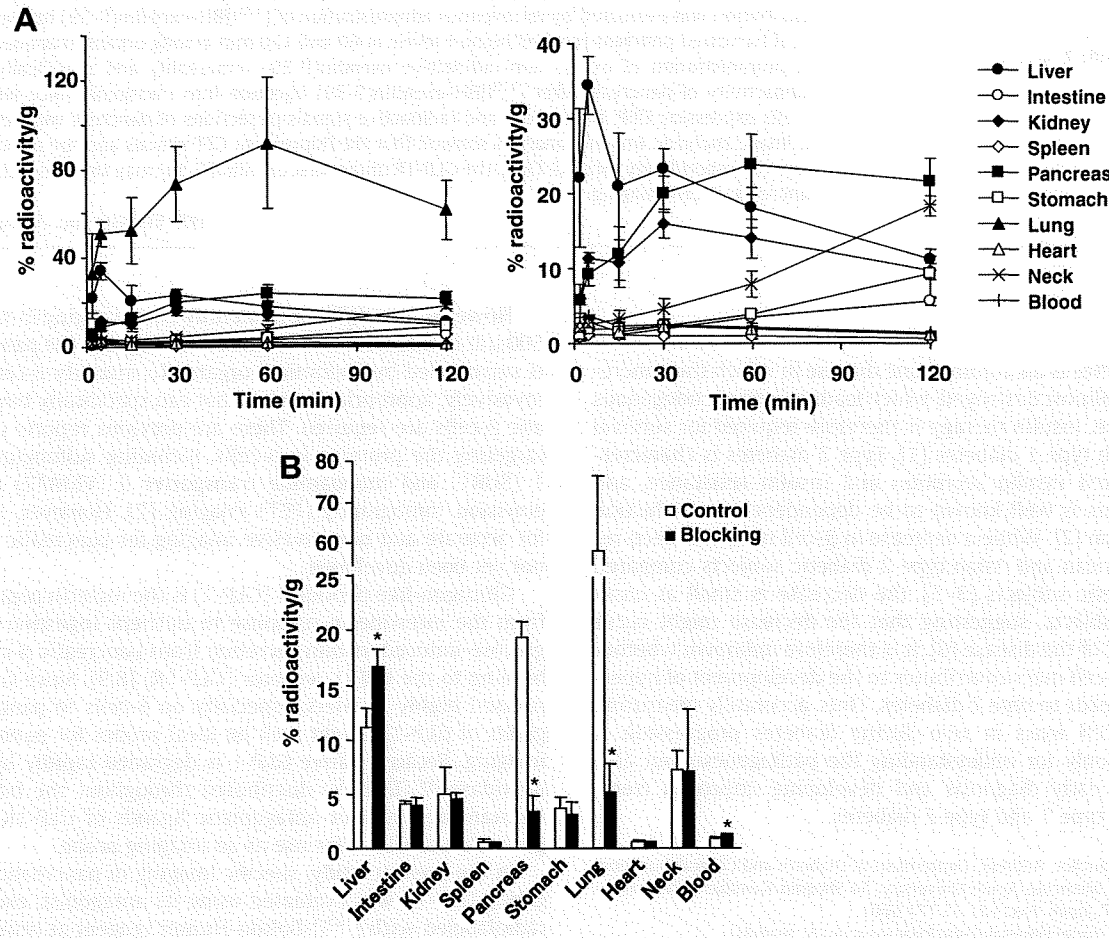

Fig. 2. Tissue distribution of [^{125}I]BH-exendin(9-39) in mice. (A) Time course of tissue distribution of [^{125}I]BH-exendin(9-39). Right graph shows tissue distribution without lung. (B) Blocking of tissue distribution at 120 min after [^{125}I]BH-exendin(9-39) injection by pre-administration of excess non-radioactive exendin(9-39). Values are expressed as means ± SD of the percent radioactivity of injected [^{125}I]BH-exendin(9-39) per gram of organ weight (n = 5). $^{*}P < 0.001$ vs. control.

were harvested and weighed, and the radioactivities were measured with a γ-counter. In a blocking study, excess non-radioactive exendin(9-39) (50 μg) in 100 μl of saline was administered 30 min before the [^{125}I]BH-exendin(9-39) injection. Results were expressed as percent radioactivity of injected [^{125}I]BH-exendin(9-39) per gram of organ weight.

Two-dimensional imaging analysis. After intravenous administration of [^{125}I]BH-exendin(9-39) to male MIP-GFP mice, the pancreas was harvested and cut in several pieces. Each piece was put on slide glass and pressed with a cover glass. Signals of fluorescence and radioactivity (autoradiography) of sections of pancreas were evaluated with an image analyzer (Typhoon 9410; GE Healthcare, Buckinghamshire, UK). The fluorescent and radioactive intensity of each section was analyzed with ImageQuant TL software with resolution of 25 and 10 μm per pixel, respectively (GE Healthcare).

Statistical analysis. Data are expressed as means ± SD. Statistical significance of difference was evaluated by unpaired alternate Welch *t* test. $P < 0.05$ was considered significant.

Results and discussion

We first examined binding specificity of exendin(9-39) to pancreatic β-cell membrane *in vitro*. Binding assay analysis using mouse pancreatic islet cells showed competitive inhibition of [^{125}I]BH-exendin(9-39) binding by non-radioactive exendin(9-39) with a $\log IC_{50}$ of -8.84 ± 0.18, similarly to the findings in a previous report [15], indicating that exendin(9-39) binds to those cells specifically (Fig. 1).

To examine selectivity of exendin(9-39) to pancreas *in vivo*, we performed biodistribution studies in mice. Radioactivities of selected organs were measured 15, 30, 60, and 120 min after intravenous administration of [^{125}I]BH-exendin(9-39) (1 μCi). The radioactivity of lung was highest at each time point (Fig. 2A, left panel). Radioactivity of pancreas increased with time and was highest at 60 and 120 min among organs examined excepting lung, and rapid and high binding by liver was observed (Fig. 2A, right panel). To determine whether the binding was specific, we performed blocking study. Pre-administration of excess non-radioactive exendin(9-39) (50 μg) significantly blocked the radioactivities of pancreas and lung to 17.8% and 8.8% of control, respectively, 120 min after [^{125}I]BH-exendin(9-39) injection (Fig. 2B), demonstrating that [^{125}I]BH-exendin(9-39) specifically binds to its receptor in these organs. The binding in other organs such as liver was not blocked by excess non-radioactive exendin(9-39).

To confirm high binding of exendin(9-39) in β-cells, we performed [^{125}I]BH-exendin(9-39) injection in MIP-GFP mice specifically expressing GFP in pancreatic β-cells and imaging analysis of sections of the pancreas removed 60 or 120 min after [^{125}I]BH-exendin(9-39) injection. As shown in Fig. 3A, fluorescent GFP signals were observed in the pancreatic sections of MIP-GFP mice with an image analyzer. Localization of the detected radioactive signals corresponded well to that of the GFP signals, indicating specific high binding of exendin(9-39) in pancreatic β-cells. The intensity of the fluorescent signals of each section also correlated with that of the radioactive signals (Fig. 3B).

Studies for detecting β-cell mass have been performed using probes targeting various β-cell-specific molecules, among which GLP-1R appears promising [7]. *In vivo* imaging of GLP-1R-positive tissues using diethylenetriaminepentaacetic acid (DTPA)-conjugated exendin-4, the GLP-1R agonist, was recently reported [16]. The biodistribution examinations showed its specific binding not only to pancreas and lung but also to stomach. Although pancreas and lung as well as pituitary and adrenals were detected in single photon emission computed tomography (SPECT) imaging, it was not determined whether the probe was confined to β-cells due to the low resolution of the imaging apparatus. In the present study, we found that exendin(9-39), an antagonistic ligand of GLP-1R, has high specificity not only to pancreas but also to β-cells in pancreas, suggesting that β-cell mass can be evaluated. High binding of the probe in lung, as previously reported [16], does not affect analysis of islets because lung is an extra-abdominal organ, for which imaging such as SPECT is required.

A better understanding of the relationship between β-cell mass, β-cell function, and glucose homeostasis by precise measurement of β-cell mass should provide important information on not only for early diagnosis and treatment but also for development of new therapies for intervention strategies. Several tests are presently available for evaluation of β-cell function [17]. In contrast,

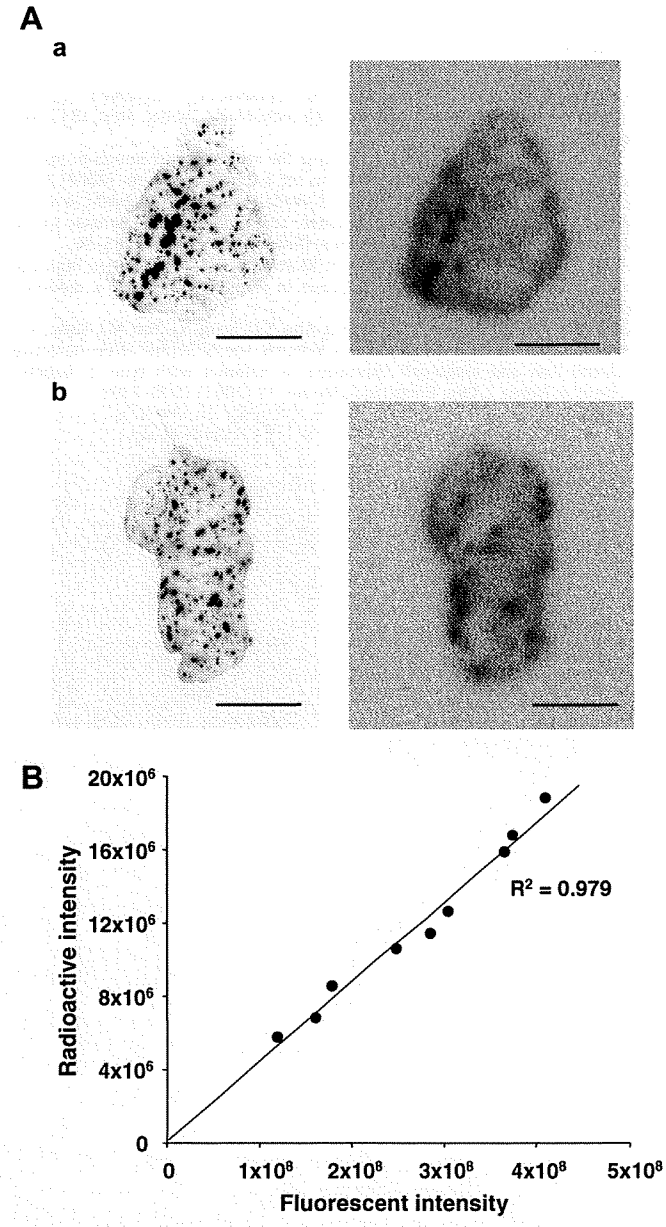

Fig. 3. Imaging analysis of pancreas sections of [^{125}I]BH-exendin(9-39)-injected MIP-GFP mice. (A) Representative fluorescent signals (left panels) and radioactive signals (right panels) of pancreas sections at 60 min (a) and 120 min (b) after [^{125}I]BH-exendin(9-39) injection. Bars represent 1 cm. (B) Correlation of the fluorescent and radioactive intensity. The signal intensity in whole area of each of the nine sections of pancreas harvested 120 min after [^{125}I]BH-exendin(9-39) injection was analyzed with ImageQuant TL software.